UNIVERSITY OF TARTU

Faculty of Science and Technology

Institute of Physics

Artene Petrică

"Energy level structure and electron – phonon coupling in the   light – harvesting complex II"

Master's thesis

Supervisor: Prof. Dr. Jörg Pieper

Tartu 2013

Table of contents

Abstract

Photosynthesis is a key biological process on our planet. Light harvesting and excitation energy transfer are the primary processes in photosynthesis. These functions are fulfilled in green plants by photosynthetic antenna systems embedded into the thylakoid membranes on the chloroplasts.

In my thesis I am studying energy level structure and electron – phonon coupling in the light – harvesting complex II, which is one of the most abundant pigment – protein complex in green plants. My experimental work is split in two major parts: first part (Chapter 3.1) describes simulations and results done with calculation routines written in Wolfram Mathematica® 8.0 (written by Prof. Dr. Jörg Pieper) and the second part (Chapters 3.2 and 3.3) concerns practical experiments and results where I used absorption, CD and ΔFLN spectroscopy on different LHC II preparations.

The ΔFLN has been compared with SHB technique from the point of view of the accuracy of the information in extracting the S – factor values (the measure of electron – phonon strength) for our pigment - protein complex.

I have showed that the electron – phonon coupling strengths values calculated were closer to the real value in the low – fluence range for ΔFLN comparing with SHB results which were significant far from the true value of 1. These results underline that ΔFLN is advantageous over SHB in determining S-factors in the low-fluence limit, while extreme care has to be taken when analysing ΔFLN and SHB spectra in dependence on fluence and excitation wavelength within the IDF.

Circular Dichroism spectra are due to the short – range excitonic coupling between chromophores. The temperature dependence spectrum of mutant samples shows a shift from the expected linear dependence of the peaks. For Chl a612 mutant (thought to be the lowest energy state of the LHC II) we could see a strong shift of the ~680 nm peak towards red region of the spectra. A structural transition might be possible to occur over ~240 K.

The temperature dependence of the system can be described by an asymmetric double well potential, where these describes two energetically inequivalent protein conformations. The system is trapped at one conformation at low temperatures and another conformation is found at elevated temperatures.

As conclusion, the protein environment might "fine – tune" the site energies of pigment molecules.

List of abbreviations

asparagine	Asn
circular dichroism	CD
chlorophyll	Chl
delta fluorescence line narrowing	ΔFLN
excitation energy transfer	EET
femtoseconds	fs
fluorescence line narrowing	FLN
full-width-at-half-maximum	FWHM
glutamate	Glu
high performance liquid chromatography	HPLC
Huang-Rhys factor	S factor
inhomogeneous distribution function	IDF
light harvesting complex II	LHC II
lutein	Lut
lysine	Lys
neoxanthin	Neo
non-photochemical hole burning	NPHB
phonon sideband	PSB
picoseconds	Ps
quasieleastic neuron scattering	QENS
reaction centre	RC
single molecule spectroscopy	SMS
signal to noise ratio	SNR
spectral hole burning	SHB
vioxanthin	Vio
water-soluble chlorophyll-binding protein	WSCP
zero-phonon line	ZPL

1.   Introduction

1.1.   Overview of photosynthesis

Photosynthesis is a key biological process on our planet. For the past 2.5 billion years nature has developed and optimized photosynthesis. It converts solar energy into storable chemical energy and provides a food source for all higher life on earth. By the photosynthetic process all fossil fuels are poduced, ozone layer is formed which protects life on earth from dangerous UV radiations and oxygen is realeased into athmosphere (Fromme, 2008).

There are two types of photosynthesis: anoxygenic and oxygenic. In this work we are going to focus on oxygenic photosynthesis. All oxygenic photosynthetic organisms use water as a universal electron donor and realease, as seconday product, oxygen into atmosphere (Fromme, 2008).

The scientific interest in Photosynthesis is very high, since understanding the structure of photosynthetic pigment – protein complexes and their function can solve the energy crisis, leading to a new era towards biological energy sources or to development of efficient artificial photosynthesis.

Light harvesting and excitation energy transfer are the primary processes in photosynthesis. In green plants, the light-harvesting complexes embeded into the thylakoid membranes of chloroplasts fulfill the function of harvesting solar energy efficiently. Generally, green plants contain two photosystems: Photosystem I (PS I) and Photosystem II (PS II).

1.1.1.   Photosynthetic antenna systems

Solar photons are absorbed by a complex system of membrane associated pigment – protein complexes (light – harvesting antennae) and the resulting excited electronic state is efficiently transferred to reaction centers (RC) located in the core of the photosystems, where charge separation takes place (Amerongen, et al., 2000).

The nature has developed different types of antenna complexes, which is why the structure of the antenna systems differs greatly between different photosynthetic species (Fromme, 2008). Generally there are two major types of photosynthetic antenna systems: extrinsic (found in cyanobacteria) and intrinsic (for all the other higher photosynthetic organisms). The intrinsic antennae systems are of two types as well: peripheral and core systems. The LHC II complex, studied in the present thesis, is part of the peripheral antenna system and is the most numerous (Ruban, 2012).

1.1.2. Structure and function of light-harvesting complex II (LHC II)

The light – harvesting complexes of the PS II consists of core complexes (CP43, CP47) and so – called peripheral antenna complexes: LHC II, CP 29, CP 26 and CP 24. From these four, the LHC II is the most abundant in chloroplasts and it is known as the major light – harvesting complex II; the other three have been named as minor light –harvesting complexes or chlorophyll binding proteins (CPs) (Liu, et al., 2004). LHC II is not serving just as an antenna complex but also plays and important role in dissipation of excess energy (photoprotection role).

LHC II binds defined amounts of chlorophyll *a* and *b*. On the other side, reaction centers have just Chl *a* as green pigment. LHC II accounts for roughly one – third of the total membrane protein in plant thylakoids (Standfuss & Kühlbrandt, 2004).

The structure of LHC II has been resolved at atomic resolution. It has been shown that native LHC II from isolated plant tissues is a trimer. The trimeric LHC II consists of three nuclear gene – products *Lhcb1*, *Lhcb2* and *Lhcb3* found in unequal stoichiometries (Standfuss & Kühlbrandt, 2004).

The monomers of LHC II are small proteins. According to recent studies, LHC II monomeric form binds eight chlorophyll *a* (Chl *a*), six chlorophyll *b* (Chl *b*), two lutein (Lut), one neoxanthin (Neo) and one vioxanthin (Vio) which are arranged for efficient light - harvesting. The Chls in LHC II are vertically distributed into two layers within the membrane. Each monomeric unit of LHC II binds five Chl *a* and three Chl *b* close to stromal surface. The other three remaining Chl *a* and three Chl *b* are placed towards the luminal surface (Liu, et al., 2004).

In LHC II, center – to – center distances of the chlorophyll molecules are rather small with an average of 11.26 Å. This density is very high and may thus cause excitonic interactions between chlorophylls, see below.

1.1.3. Electron-phonon coupling and energy transfer in photosynthesis

There are three types of interactions that affect the shape of the absorption spectrum of pigment-protein complexes and promote excitation energy transfer between chlorophylls:

a) pigment – protein interaction determining the electronic transition energy of the pigment molecules; b) pigment – pigment interaction (or excitonic) which is further tuning the transition energy of the pigment molecules, but may also lead to a redistribution of their absorption intensities and c) electron – vibrational interaction.

In LHC II the distance between chlorophylls are so small that excitonic interactions between them are inevitable. There are many attempts for calculating the excitonic coupling between two chlorophylls, which are largely based on results of various spectroscopic techniques and fitting procedures (Fromme, 2008).

To start with, an exciton is a bound state of an electron and a hole which can transfer energy without transporting net electric charge (Pieper & Freiberg, In press). The whole antenna complex is characterized by an intricate structure of the excited states (excitons) with a high degree of delocalization in sequence with more localized excitations caused by the presence of weakly coupled pigments (Grondelle & Novoderezhkin, 2005).

Photosynthetic antenna complexes display electron – vibrational coupling as well. The electron – vibrational coupling is defined as an interaction between the electronic transition of pigment molecules and the inter- as well as intramolecular nuclear vibrations.

The electron – vibrational coupling defines the vibronic structure of an individuals' pigment optical spectrum (Vrandecic, 2013). In native antenna complexes excitations are coupled to a continuum of delocalized low frequency protein vibrations (also referred to as phonons) peaking at about $20 - 30 \text{ cm}^{-1}$ and to several more localized vibrational modes of the pigment molecules with frequencies up to 1700 cm^{-1} allowing energy transfer from the higher to lower – energy states (Grondelle & Novoderezhkin, 2005).

If an electronic transition occurs without change in the phonon levels population it is called *zero – phonon transition*. Zero – phonon transitions form zero – phonon lines (ZPL) in optical spectra. Further transition can generate certain numbers of phonons, and are respectively referred to as one - , two - or n – phonon transitions. Within the Frank – Condon approach, the heavy nuclei do not react during a fast transition upon light absorption.

Spectral features connected to the change in population of phonon levels are referred to as the phonon sideband (PSB). The average number of phonons associated with a particular electronic transition is measured by Huang – Rhys factor S (Pieper & Freiberg, In press). . The theory of electron – phonon coupling discussed within this work is strictly valid for highly localized electronic transitions only, see below.

The homogeneously broadened spectra of photosynthetic antenna complexes is composed of the life-time broadened ZPL and features due to electron – phonon and electron – vibrational interactions. The coupling of electronic excitations to slow conformational changes of the antenna produces further changes in a pigment's absorption frequency viewed as

inhomogeneous broadening. The dynamics of this conformational changes can be studied using Spectral Hole – Burning, Single – Molecule Spectroscopy or other line – narrowing spectroscopic techniques (Grondelle & Novoderezhkin, 2005). In conventional spectroscopies, the presence of inhomogeneous broadening leads to rather structureless optical spectra.

1.1.4. Current studies in literature

Different spectroscopic techniques have been applied to study light harvesting and EET in LHC II, for example: single molecule spectroscopy (SMS), fluorescence line – narrowing spectroscopy (FLN), difference fluorescence line – narrowing spectroscopy, absorption spectroscopy, spectral hole – burning (SHB), linear dichroism (LD), circular dichroism (CD) or time – resolved absorption spectroscopy (TA). The availability of the high – resolution X - ray structure of LHC II made the interpretation of this data easier. But there are still many uncertainties regarding allocating the site energies, excitonic coupling strengths and excitation energy transfer (EET) pathways.

Time – resolved studies indicate that Chl $b \rightarrow$ Chl a EET within LHC II occurs on fs – and ps – timescales. Excitation dynamics have been modelled at a quantitative level and such simulations helped to find structural assignments of certain rates to specific energy transfer pathways from certain chlorophylls to others. Van Grondelle and Novoderezhkin (2005) have modelled an energy level diagram together with relaxation time constants for LHC II monomer (Grondelle & Novoderezhkin, 2005).

It is a challenging task to determine the energy level structure and to reach a structural assignment of excitation dynamics. A quantitative description of energy transfer is possible only by using a realistic exciton – phonon spectral density and by including multi – phonon processes.

It is known that Chl b is responsible for the absorption at wavelengths in the vicinity of ~650 nm and the absorption in the range of ~670 – 680 nm is due to Chl a (Lichtenthaler, 1987). The interaction between chlorophylls plus the pigment – pigment, pigment – protein and pigment – vibrational interactions modify the shape of the absorption spectrum. The absorption bands peaks of all the 42 Chl of LHC II are hidden by significant inhomogeneous broadening and only 4 Qy – absorption bands can be distinguish at 4.2 K (Vrandecic, 2013).

Van Grondelle et. al. (2005) have conducted experiments and simulations on EET for LHC II at 77 K. They modelled EET in monomeric LHC II at a quantitative level based on results of time –resolved spectroscopy. The timescale and pathways of EET were discussed (Figure 1).

In this study, the importance of random shifts induced by slow conformations is pointed out as a major factor in determining the excitation dynamics. The energy level diagram for the LHC II monomer is composed by three major kinetic groups (clusters): fast excitonic relaxation occurs within clusters (fs) and slower EET transfer between clusters (ps). According to this study the lowest energy state is located on a domain of three excitonically coupled Chl a molecules including Chl *a*610, 611 and 612 (Grondelle & Novoderezhkin, 2005).
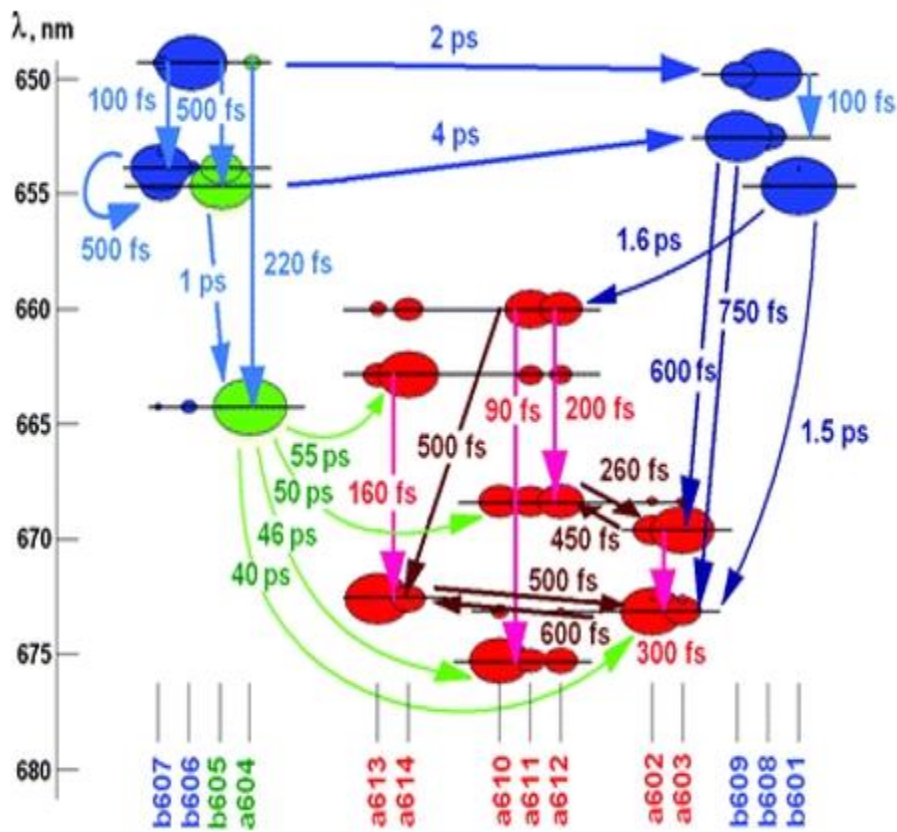

Figure 1. Energy-level diagram for a single monomeric LHCII complex. The positions (wavelengths) of the 14 exciton levels, participation of the pigments in these exciton states, and relaxation time constants are shown for one typical realization of the disorder. Three groups of kinetics show populations of the *b*-sites with fast decay (blue), *a*-sites which contribute to the main absorption peak near 675 nm (red), and long-lived 'bottleneck' sites (green), *i.e.* blue-shifted Chl *a* (*a*604) and red-shifted Chl *b* (*b*605). [*Accessed on 12.05.2014/5pm; Permission granted*].

Later, researchers have combined quantum chemical and electrostatic approaches to calculate excitonic couplings and site energies applied to Qy transition of Chl in trimeric LHC II from plants based on the high – resolution crystal structure. One of these results is also saying that the lowest energy state is located on Chl *a*610 (Müh, et al., 2010).

Pieper et. al. (2009) have analysed and compared trimeric and monomeric LHC II samples with SHB and FLN at 4.2 K reaching to challenging conclusions. Pigment – pigment coupling

strengths and assignment of low energy excitonic states were addressed. The lowest Qy state resulted to be widely localized on one Chl *a* molecule, which is possibly in close contact to a Chl *b*, but rather isolated from other Chl *a* molecules. Because of the high degree of localization, the lowest energy state at about 679.6 nm was assumed to Chl *a*604, which is the only Chl *a* molecule without close contact to other Chls *a* (Pieper, et al., 2009).

Rogl et. al. (2002) had showed that spectral bands in the absorption spectrum of LHC II can be assigned to individual Chl molecules located at well - defined binding sites using mutant LHC II samples. These were recombinant forms of LHC II where a specific Chl was removed from its binding site by site – directed mutagenesis. However, only four mutations of Chl – binding sites led to stable complexes that could be spectroscopically studied (Figure 2). They also found that the sub – band position of Chl *a*612 may be the energetically lowest at room temperature, but reveals a temperature dependent spectral shift (Rogl, et al., 2002).
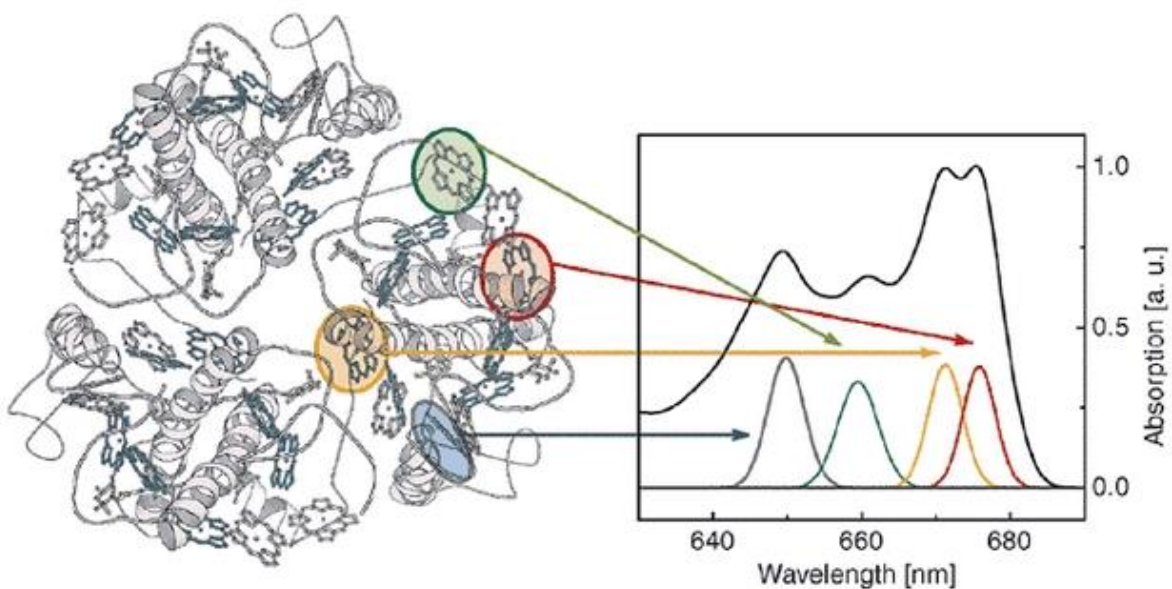
Figure 2. Assignment of spectral chlorophyll forms to the corresponding binding sites in the 3D structure of LHC-II: Chl b6, blue; Chl b3, green; Chl a5, yellow; Chl a2, red. The LHC-II trimer is viewed from the stromal side. [*Accessed 12.05.2014/5pm; Permission granted*]

QENS studies revealed an onset of protein conformations around 77 K for native LHC II. This protein dynamics might affect excited state positions in LHC II (Vrandecic, et al., 2014).

Photoprotection, nonphotochemical quenching (NPQ) and spectral assignment of chlorophylls were discussed by Jörg Standfuss et. al. (2005) based on the crystal structure on LHC II. Their results suggested that the NPQ has two components: conversion of Vio to Zea in the xanthophyll cycle and a drop in pH (Standfuss, et al., 2005).

In summary, there is still a large uncertainty in the structural assignment of the LHC II site energies and in the proper understanding of EET in general.

Therefore, the purpose of this thesis is to address the following aspects: the energy level structure and electron – phonon coupling in the light – harvesting complex II by using simulations, selective optical spectroscopies and Circular Dichroism techniques. In a more detailed view I will discuss:

- Advantages of ΔFLN technique over the other selective spectroscopic techniques;
- The dependence of the Huang Rhys factor on excitation wavelength and fluence using ΔFLN technique for wild type (Lhcb1) and mutant LHC II samples (Chl *a*612 and Chl *a*610) ;
- Temperature – dependent absorption spectra of mutant LHC II samples lacking certain pigment molecules compared with the intact LHC II sample;
- Temperature – dependent CD spectra of wild type (Lhcb1) and mutant LHC II samples (Chl *a*612 and Chl *a*610);
- The potential energy diagram in the vicinity of Chl *a*612 (lowest energetic state of LHC II complex).

The present thesis is based on analysing wild type and mutant LHC II samples, as well as computational modelling, using a well-studied complex with known parameters.

2.   Methods and samples

In this chapter I will present the background of the techniques used in my experiments: SHB, FLN, delta FLN and CD. Also, information about sample preparation and instrumental setups for the experiments will be detailed in the coming sub-chapters.

2.1.   Selective spectroscopic techniques applied on LHC II

A single molecule spectrum is by definition a homogeneously broadened spectrum of a pigment molecule embedded into a protein matrix. In case of the LHC II complex (mix of pigments embedded into protein matrix) we encounter inhomogeneously broadened spectra (information is hidden by the inhomogeneous broadening) because of the different protein environment of each chemically equivalent pigment molecule in a bulk sample which affects the transition frequency of the molecule in a different way. Therefore, there is a need for techniques that can remove the inhomogeneous broadening which will be discussed more detailed into coming section.

The homogeneously broadened spectrum of a pigment molecule in a pigment-protein complex consists of ZPL and PSB, if its electronic transition couples to protein vibrations. The transition probabilities is given by Frank − Condon principle and follows the equation:

$$W_{fm,in} = \left| D_{f,i} \prod_k \langle m_k | n_k \rangle \right|^2$$

where: $D_{f,i}$ = elctronic transition probabilities f, respecctively i

m_k, n_k = vibrational levels n and m

The homogeneously broadened spectra can be described using the following equation:

$$L_\omega = e^{-S} l_0(\omega - \Omega) + \sum_{R=1}^{\infty} S^R \frac{e^{-S}}{R!} l_R(\omega - \Omega \pm R\omega_m)$$

where: $-R\omega_m$ = Absorption

$+R\omega_m$ = Fluorescence

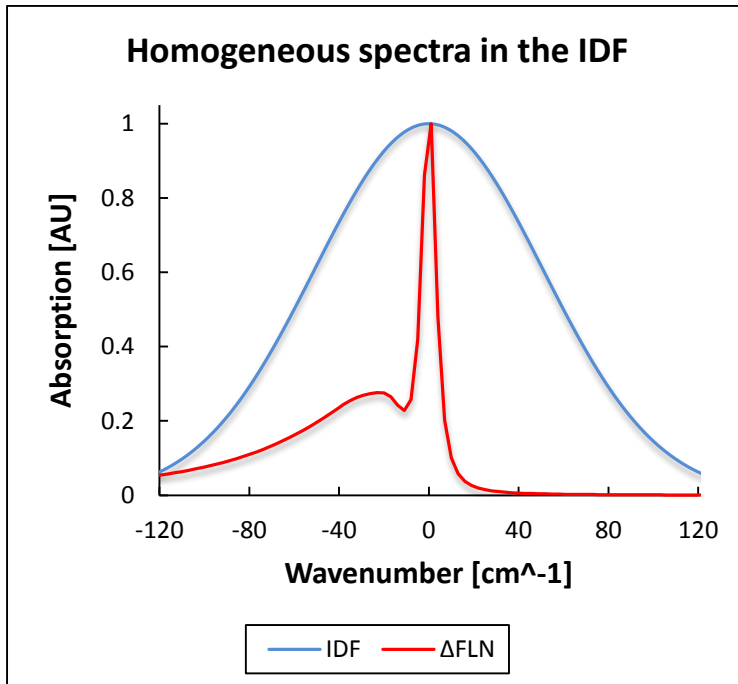$l_R(\omega - \Omega_0 \pm R\omega_m)$ = one phonon profile

S = Huang − Rhys factor

$R!$ = total number of phonon transitions

The first term describes ZPL having a Lorentzian shape l_0 at frequency Ω. The PSB consists of all l_R terms with R=1, 2, 3… corresponding to one-phonon (R=1) and multiphonon (R≥2)

transitions. The Huang-Rhys factor S characterizes the number of phonons accompanying a particular electronic transition.

However, for an ensemble of similar pigments (chromophores), we observe broad and structureless spectra. The reason for this is inhomogeneous broadening due to the irregular protein environment of each chlorophyll (Figure 3). The structure of the protein surrounding the pigments differs from pigment to pigment which affects the transition frequency of that particular molecule so that it differs from complex to complex in a bulk sample.

Figure 3: Homogeneously broadened spectrum in the IDF (ΔFLN spectrum).

The inhomogeneously broadened spectrum calculated in the low fluence limit can be described in a mathematical way using the following equation:

$$L(\omega) = \sum_{R=0}^{\infty} \left(S^R \frac{e^{-S}}{R!} \right) \int d\Omega_0 N(\Omega_0 - \omega_C) l_R (\omega - \Omega_0 \pm R\omega_m)$$

where: $-R\omega_m$ = Absorption

$+R\omega_m$ = Fluorescence

$N(\Omega_0 - \omega_C)$ = Gaussian IDF

$l_R(\omega - \Omega_0 \pm R\omega_m)$ = one phonon profile

S = Huang − Rhys factor

R = total number of phonon transitions

This static inhomogeneous broadening can be described using a Gaussian function with full widths of $80 - 200\text{cm}^{-1}$ which is called inhomogeneous distribution function (IDF) see blue line in Figure 3. The IDF determines the spectral resolution in conventional spectroscopy (Pieper & Freiberg, In press). For comparison a homogeneously broadened spectrum with narrow ZPL and broad PSB is also shown in Figure 3.

Conventional absorption and fluorescence techniques are largely structureless as the inhomogeneous broadening makes it difficult to see the optical transmissions of the individual pigments.

To overcome these difficulties in analysing pigment – protein complexes and for a better understanding of the photosynthesis mechanism, line – narrowing techniques can be used together with CD or time – resolved spectroscopy.

All line – narrowing techniques are based on selective laser excitation, which selects information from only a subset of pigment molecules absorbing at a certain burn/excitation frequency.

2.1.1. Spectral hole burning (SHB)

Hole – burning spectroscopy was first discovered in 1980's thanks to the work of two research groups: Bykovskaya (Kharlamov, et al., 1974) and Gorokhovskii, Kaarli and Rebane (Gorokhovskii, et al., 1974). Nowadays, the field expanded enormously and this technique is also used in studying biological systems as: reaction centers or antenna protein complexes.

Hole – burning spectra are defined as the difference in absorbance before and after burning with the selective laser wavelength. In other words, the difference between absorption spectrum at burn frequency ω_B at the burn time t and the pre-burn absorption spectrum at the start of the experiment in the low fluence limit can be described using the following equation:

$$\Delta A(\omega) = \sum_{R,P=0}^{\infty} (S^R \frac{e^{-S}}{R!})\left(S^P \frac{e^{-S}}{P!}\right) \int d\Omega_0 \, N(\Omega_0 - \omega_C) \times l_P(\omega_B - \Omega_0 - P\Omega_m) \times l_R(\omega - \Omega_0 - R\omega_m)$$

where: l_p = electronic transitions bleached during the burn process

$-R\omega_m$ = absorption
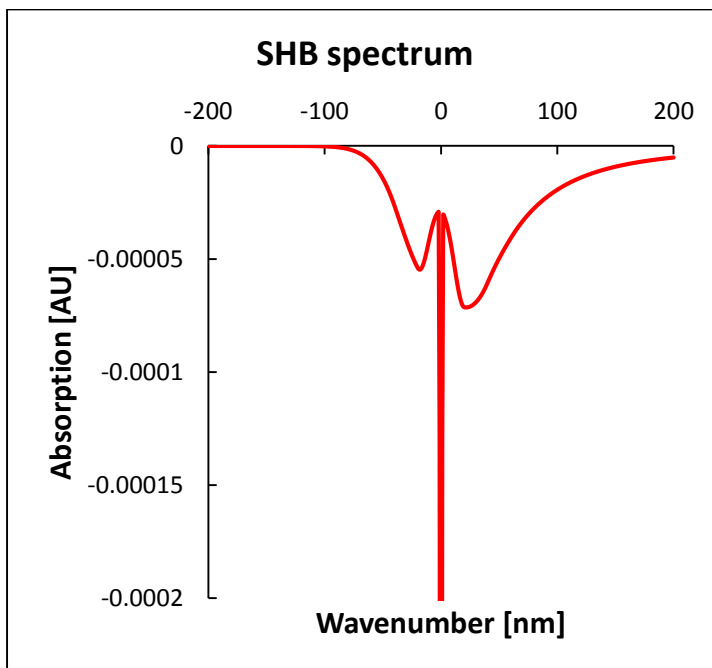
S = Huang − Rhys factor

ω_C = position of the IDF

ω_m = peak phonon frequency

ω_B = laser light frequency

$N(\Omega_0 - \omega_C)$ = Gaussian IDF

SHB can provide valuable data on the underlying structure of the absorption profile of a pigment embedded into a heterogeneous protein matrix even in case of strong linear electron – phonon coupling. A calculated SHB spectrum is shown in Figure 4 and it shows a strong zero – phonon line (ZPL) due to resonantly burned electronic transitions overlapping the burn frequency ω_B. The other two features are pseudo phonon sideband (pseudo –PSB) which is due to non - resonant overlap to the burn frequency and real phonon sideband (real – PSB) which arises from the PSBs of the resonantly bleached electronic transitions at the selective burn frequency (Pieper & Freiberg, In press).

Figure 4: SHB spectrum (modelled).

Accurate extraction on Huang – Rhys factors is hard to obtain in such a systems where the width of the PSB is identical or even larger that of the IDF. The real – PSB of the SHB spectra is often interfered with by the anti – hole. Therefore, the one – phonon profile is obtained from the more intense pseudo – PSB (Pieper & Freiberg, In press).

2.1.2. Fluorescence line-narrowing (FLN)

The fluorescence line – narrowing technique is complementary to SHB in the analysis of pigment – protein complexes and it is a non – destructive technique. Similar with SHB, FLN it allows for the elimination of inhomogeneous broadening and it can be expressed in a similar form in the low temperature region:

$$F(\omega) = \sum_{R,P=0}^{\infty} (S^R \frac{e^{-S}}{R!}) \left(S^P \frac{e^{-S}}{P!} \right) \int d\Omega_0 \, N(\Omega_0 - \omega_C) \times l_P(\omega_B - \Omega_0 - P\Omega_m) \times l_R(\omega - \Omega_0$$
$$+ R\omega_m)$$

where: l_p = electronic transitions bleached during the burn process

$+R\omega_m$ = fluorescence

S = Huang − Rhys factor

ω_C = position of the IDF

ω_m = peak phonon frequency

ω_B = laser light frequency

At low temperature the individual line shape of a single site spectrum consists of a zero-phonon line (ZPL) and only a single PSB feature because the real – PSB is superimposed on the pseudo – PSB on the low energy side.

2.1.3. Delta fluorescence line-narrowing (ΔFLN)

Thanks to early pioneer works of Jaanisoo (1985) and Fünfschilling et al. (1986) and further improvements added by Rätsep and Freiberg (2007) a relatively new method appeared called delta fluorescence line – narrowing (ΔFLN). In analogy to SHB it is defined as the difference of FLN spectra measured before and after an intermediate hole-burning step. This method is capable to solve the difficulties of the other two methods discussed above and electron – phonon and electron – vibrational coupling strengths can be determined directly (Pieper & Freiberg, In press). The ΔFLN spectra is obtained by subtracting pre – and post – burn FLN spectra and it can be expressed mathematically with the following equation:

$$\Delta FLN(\omega) = ke^{-3S} \sum_{R,P=0}^{\infty} \frac{S^Q}{Q!} \frac{S^R}{R!} \frac{S^P}{P!} \int d\Omega_0 N(\Omega_0 - \omega_C) \times l_Q(\omega_E - \Omega_0 - Q\omega_m) \times l_R(\omega_B - \Omega_0$$
$$- R\omega_m) \times l_P(\omega - \Omega_0 + P\omega_m)$$

where: ... l_p = electronic transitions bleached during the burn process

$+P\omega_m$ = fluorescence

S = Huang − Rhys factor

ω_C = position of the IDF

ω_m = peak phonon frequency

ω_B = laser light frequency

ΔFLN enhances two important advantages comparing to SHB and FLN spectroscopy: the scattered light which affects the FLN spectra can be eliminated through the difference spectra and in the low – fluence limit the multiplication of l_R with l_Q leads to an enlargement of the ZPL and a suppression of the non – resonant excitation of the pseudo – PSB (Jaanisoo, 1985 and Fünfschilling et al., 1986)

In Figure 5 we can observe a ΔFLN spectrum composed by an intense ZPL and a single PSB, which is virtually identical to the homogeneously broadened fluorescence spectrum in the low fluence limit.
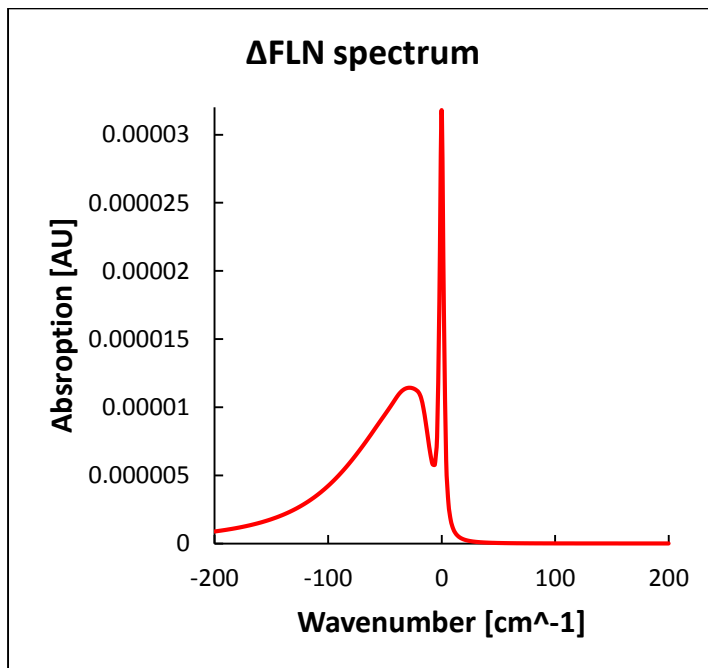

Figure 5: ΔFLN spectrum (modelled).

2.2.   Circular Dichroism (CD)

As mentioned in Section 2.1 there are numerous techniques that have been used to investigate LHC II. CD can give insights of molecular organization of pigment systems at different levels of complexity (Garab & Amerongen, 2009).

CD is defined as the difference in absorption of the left – and right – handed circularly polarized light which arises from the intra – and intermolecular asymmetry of the molecular structure. CD spectra are generally composed of three different features: a) excitonic contributions, b) intrinsic contributions due to chirality of the molecule under investigation, and c) contributions from chirality in a long – range order of larger molecular assemblies.

In molecular complexes CD is often caused by short – range excitonic coupling between chromophores which originates from the fact that the polarization of the light modifies while passing through the excitonically interacting molecules (Garab & Amerongen, 2009).

For photosynthetic complexes the CD spectra are, in practice, non – conservative which means that the sum of the positive and negative bands of the split spectrum, plotted on the energy scale, are present but not with equal area. The interpretation of the CD spectra is difficult because of the significant intrinsic CD signal leading to non – conservative spectra in the Chl b region (Müh, et al., 2010).

In our experiments we will see that the CD spectrum will change its band shape when removing one of the Chl comparing to the wild type LHC II, mainly caused by a change in the excitonic coupling between chromophores. These changes linked to the molecular structure and its energy levels will be shown and discussed in Chapter 4.

2.3.   Sample preparation and measurements

The term "LHC II mutant" refers at an LHC II complex where one of its Chl is missing. By site – directed mutagenesis the axial ligand for a specific Chl is removed, then refolding in presence of Chls leads to formation of a complex lacking one Chl (Rogl & Kühlbrandt, 1999).

There are three different nomenclatures used in literature for Chl labelling in LHC II as seen in Table 1.

Chl type	(Kühlbrandt, et al., 1994)	(Liu, et al., 2004)	(Standfuss, et al., 2005)
a	*a*1	610	Chl 1
a	*a*2	612	Chl 2
a	*a*3	613	Chl 3
a	*a*4	602	Chl 4
a	*a*5	603	Chl 5
a	*a*6	604	Chl 6
a	*b*2	611	Chl 7
a	*b*3	614	Chl 8
b		601	Chl 9
b	*a*7	607	Chl 10
b	*b*1	608	Chl 11
b	*b*5	609	Chl 12
b	*b*6	606	Chl 13
b		605	Chl 14

Table 1: Nomenclature of Chl Molecules in LHC II

The nomenclature used in the present work is according to Liu et.al., 2004.

In the present thesis two LHC II mutants used: Chl *a*612 which lacks Chl *a*612 from its composition and Chl *a*610 which lacks Chl *a*610 from its composition. *In vitro* refolding of wild type and mutant LHC II samples has been carried out following the procedure described by Rogl and Kühlbrandt (1999) (Rogl & Kühlbrandt, 1999). The reconstituted mutants were obtained by washing the prepared Escherichia Coli with buffers containing lipid, detergent and pigments with a mix of chlorophylls a/b ratio of 1.35. Wild type LHC II samples contained all Chl binding sites present in LHC IIand were thus reconstituted with all 14 chlorophylls per monomer.

For experiments the following samples were used: one wild type LHC II sample, one LHC II mutant Chl a610 and one LHC II mutant Chl a612. Samples were prepared by Laura Wilk in the laboratory of Professor Werner Kühlbrandt at Max Planck Institute Frankfurt, Germany.

During my experiments a laboratory journal was kept and some of the parameters were noted down: date, instrument, temperatures, sample, cuvette type, spectral range, bandwidth, objective, changes that occurred (e.g. lamp replacement) etc.

2.4. Setup for CD and measurements

The optical measurements of the intact LHC II and mutants were performed by me in the laboratory of Biophysics at the University of Tartu, under the supervision of Prof. Jörg Pieper and Dr. Margus Rätsep. The instrument used for absorbance and CD measurements was a ChirascanPlus spectrometer (Applied Photophysics) equipped with a CCD detector and with liquid Nitrogen Cryostat (Oxford Instruments). Absorbance measurements were taken simultaneously with the CD measurements in the range of 400 – 750 nm, bandwidth of 1 nm and step size of 0.5 nm. The temperature range was from 78 K (Kelvin degrees) to 290 K with different intermediary steps in between.

Plastic cuvettes of polymethyl methacrylate (PMMA) of 10 mm diameter were used as sample containers for absorption and CD experiments.

2.5. Setup for ΔFLN measurements

ΔFLN measurements were done with a spectrograph (Shamrock SR-303i) in the laboratory of Dr. Margus Rätsep, laboratory of Biophysics at the University of Tartu at $4.5 \pm 0.1K$. The detector used was a CCD camera (DV420A-OE, Andor Technology, U.K.) with an electrical cooling system. Spectral gratings with 600 and 1799 grooves/mm which gave a spectral resolution of 0.4 and 0.1 nm respectively. All measurements were performed into a He-bath cryostat (Utreks, Ukraine), where the sample cuvettes were kept above the level of liquid helium.

Laser fluence is a measure used to describe the energy delivered per unit area (1 cm²) and the unit used was J/cm².

3. Experimental results

My experimental work is split in two major parts: first part (Chapter 3.1) describes simulations and results done with calculation routines written in Wolfram Mathematica® 8.0 (written by Prof. Dr. Jörg Pieper) and the second part (Chapters 3.2 and 3.3) concerns practical experiments and results where I used absorption, CD and ΔFLN spectroscopy on different LHC II preparations.

3.1. Comparison of evaluation of SHB and ΔFLN spectra

Both SHB and ΔFLN techniques are useful for analysing electron – phonon coupling at low temperatures (Pieper, et al., 2009). In the scientific literature there are different opinions regarding these two techniques.

In the present thesis I would like to discuss the problems that we encounter when analysing the spectra and the advantages of ΔFLN over SHB. Three situations are discussed in the next chapters: the influence of inhomogeneous broadening on SHB line shapes, contribution of non – resonant excitation to the ΔFLN spectra and comparison of extracted S – factors from ΔFLN and SHB experimental data.

Using the model equations provided in Section 2.1.1. and 2.1.2, calculation programs to simulate SHB and ΔFLN spectra were written in Wolfram Mahematica 8.0. The inhomogeneous broadening is taken to be a Gaussian having a width of $100 \mathrm{cm}^{-1}$ and the one phonon profile was modelled with a Gaussian shape at its low – energy side and a Lorentzian shape at its high – energy side. Parameters fitted were realistic and are close to existing experimental results for the LHC II complex. The parameters used have the following values as seen in Table 2:

| Theoretical model		
Parameters	Abbreviations in Mathematica routine	Values
Huang - Rhys factor	hr	1
Gaussian PSB width	gssphwdt	20
Lorentzian PSB width	ltzwdt	60
IDF width	inhwdt	100
Zero-Phonon Line width	zplwdt	1
Excitation peak	excpeak	0

Table 2: Parameters fitted for our simulations into Mathematica routine calculation

3.1.1. Influence of inhomogeneous broadening on SHB line shapes

The first simulation conducted was to find out the influence of the inhomogeneous broadening on the SHB spectrum. All the parameters were left untouched and just the inhomogeneous width was modified from 40 cm^{-1} to 150 cm^{-1} with different intermediary steps.

In theory, the pseudo –PSB and real – PSB of SHB spectra in low – fluence region there are assumed to be mirror symmetric when the inhomogeneous width is much larger than one – phonon profile. We can see from Figure 6 how different inhomogeneous widths affect the SHB absorption spectra. As our one phonon – profile is 80 cm^{-1}, even when the inhomogeneous width is 150 cm^{-1} the both phonon side - bands are not symmetric. The flipped real – PSB should give us the impression how the pseudo – PSB had to look like in reality.

For systems where IDF is narrower comparing to PSB, the Huang – Rhys factors would be artificially lowered when the S – factor is calculated from the areas of ZPL and pseudo – PSB.
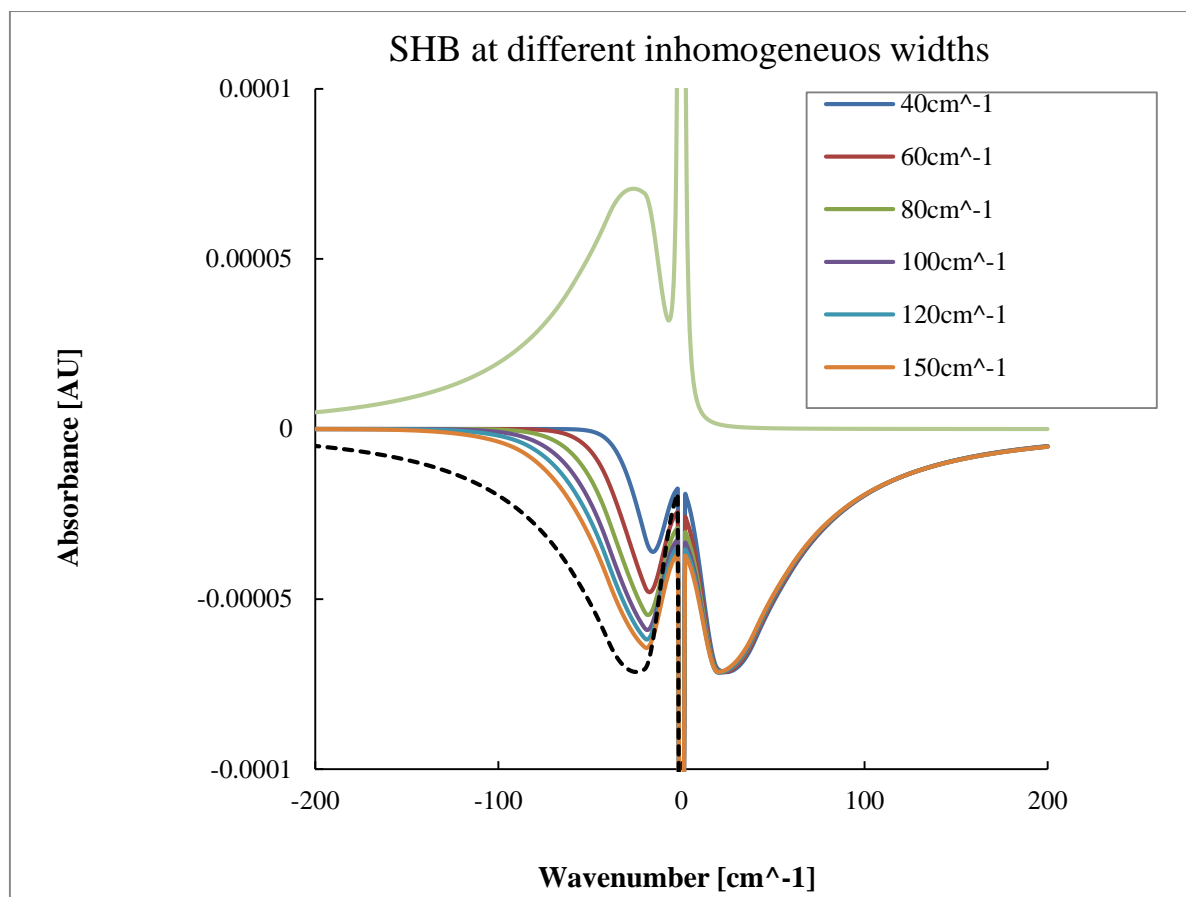
Figure 6: Simulated SHB spectra for different inhomogeneous widths

3.1.2. Contribution of non-resonant excitation to ΔFLN spectra

As seen in Section 2.1.3., in theory the ΔFLN technique with the "double selection" suppresses the pseudo – PSB in the low – fluence region and so the ΔFLN spectrum becomes identical to the homogeneously broadened spectrum. Now, trying to test this characteristic we run calculations to see how the ΔFLN spectra modify with the increase of fluence, how the pseudo - PSB contribution to ΔFLN modifies and what are the Huang –Rhys factors that we can extract.
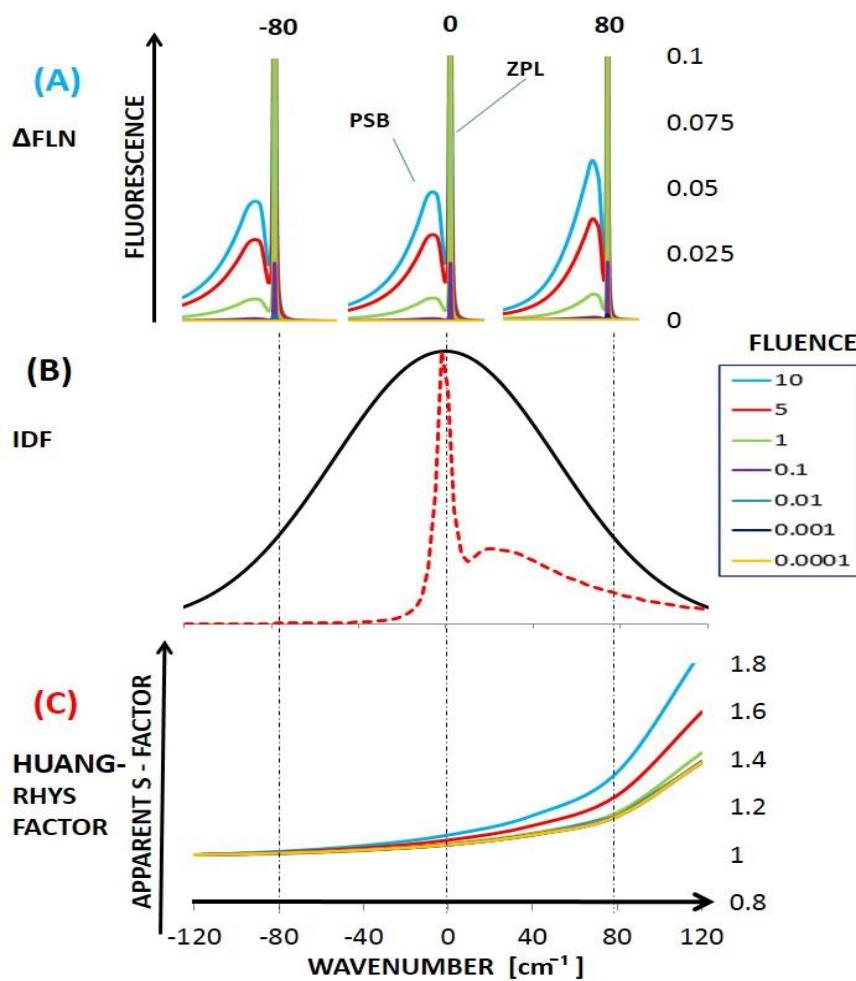
Figure 7: Simulations of ΔFLN spectra and fitting of the corresponding S – factors with fluence and excitation wavelength dependence.

Figure 7, panel (A) shows ΔFLN spectra for different fluences and different position within the IDF. It can be seen that the non – resonant contribution to the ΔFLN spectra is increasing towards higher excitation energy within the inhomogeneous distribution function (IDF) as shown in panel (B). This contribution would lead to an artificial increase in Huang – Rhys factor calculated from fits of measured data. For low – fluence limit the contribution of non –

resonant excitation to the ΔFLN spectra is almost not distinguishable in the low energy part of the IDF, while at the high energy part the expected S – factor can lead to an increase to 1.4 bigger than the real S – factor of 1 (C), according to our set of parameters (Chapter 3.1). This contribution has to be taken into account when determining S – factors from measured data and a correction is necessary for different fluences and excitation peaks. The graph provides us a real help for setting the contribution levels of the non – resonant excitation in ΔFLN spectra.

3.1.3.   Comparison of apparent S-factors extracted from SHB and ΔFLN spectra

In order to compare the capabilities of SHB and ΔFLN, apparent S-factors were extracted from spectra simulated for the fixed parameters compiled in Table 1. The two selective techniques show different results when determining the S – factors, even in low – fluence limit where, theoretically, the contribution of non – resonant excitation to the spectrum (for ΔFLN spectra) should be close to 0 (Reppert, et al., 2010). . Based on this I fitted the S – factors with our calculation rutine in Mathemathica 8.0 from the intensity ratio of ZPL and the sum of ZPL and PSB.
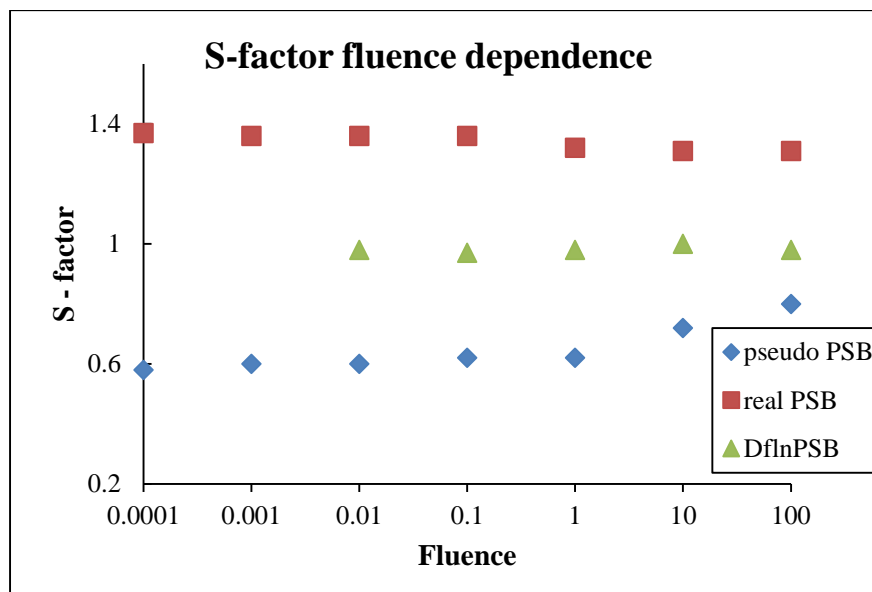
Figure 8: Expected S – factors extracted from SHB and ΔFLN experimental spectra (±0.2)

Apparent S – factors obtained from the simulated data are presented in Figure 8. The main idea was that by fitting the simulated data we should get back the same parameter (S=1) introduced at the biggining of the simulations.

Normally, with the SHB technique, the S – factor is calculated from the ZPL and pseudo- PSB intensity ratios. In this case we found that the S – factor found from fitting simulated data is underestimated and its value is rising towards higher fluence rates and it doesn't intersect with the real S – factor of 1. This effect is caused by the dependence of the pseudo – PSB intensity

on the inhomogeneous broadening width, as seen in the section 3.1.1. which affects the determination of S − factor. Also, the increase in the calculated S − factor towards the higher fluence range is due to the non − resonant contribution increasing with fluence.

In case we use the real − PSB and the ZPL to calculate the S − factor, the results will be overestimated and it shows values around 1.3 − 1.4 in the whole fluence range. The fitted result it is not close to the real one. The calculated S − factor is higher caused probably by the multi − phonon contribution to the real − PSB spectrum.

In the third case I have fitted the S − factors on the ΔFLN experimental data. Here, we can observe the advantages of ΔFLN in fitting the Huang –Rhys factors. The non − resonant contribution is suppressed due to the "double selection effect". The results were according to the real S − factors under the uncertainty of spectra fitting of ±0.2.

These results underline that ΔFLN is advantageous over SHB in determining S-factors in the low-fluence limit, while extreme care has to be taken when analyzing ΔFLN and SHB spectra in dependence on fluence and excitation wavelength within the IDF.
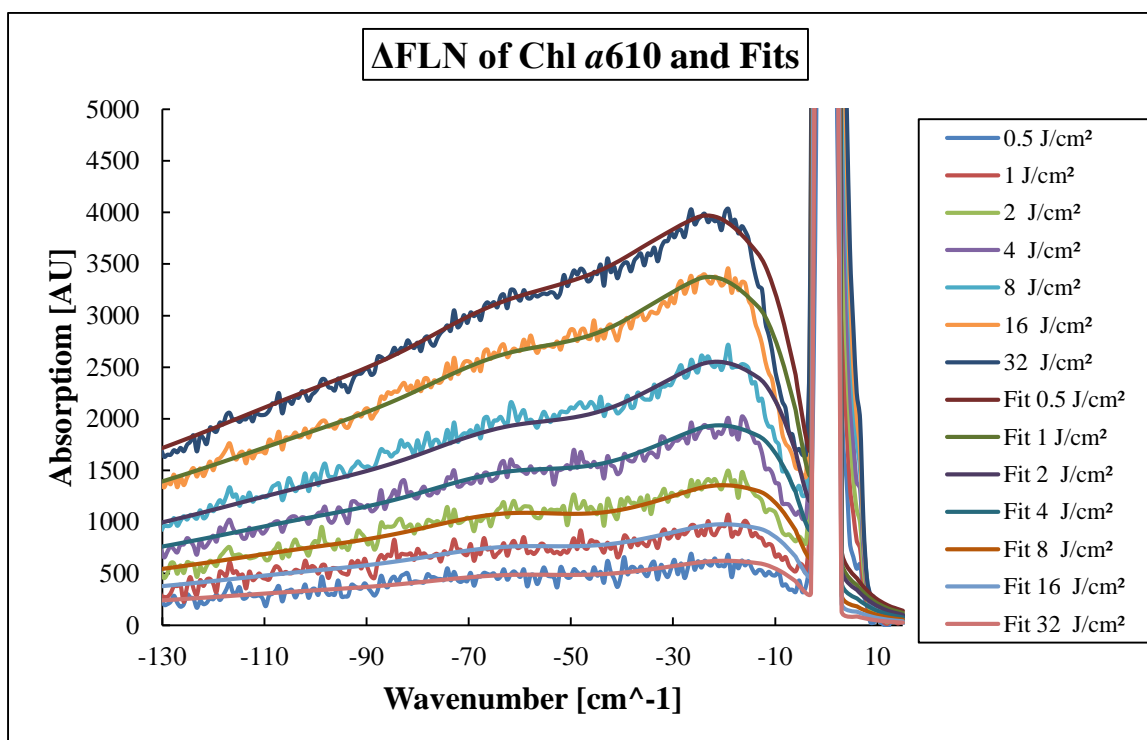
3.2. ΔFLN spectra of LHC II

In this chapter we will show the results about the influence of the different fluences and excitation wavelengths on the S-factors extracted from ΔFLN experimental spectra (Figure 9, 10 and 11 ~ one fitting example for each sample) on mutants and wild type LHC II samples.
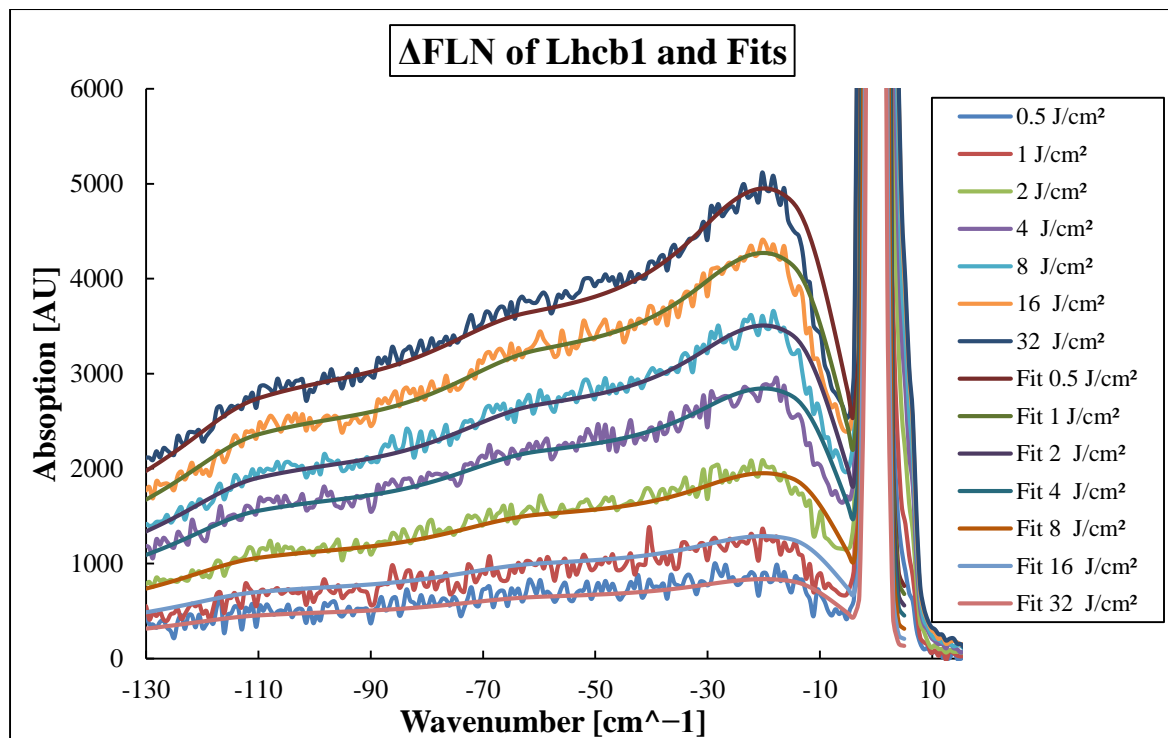
Figure 9: ΔFLN spectra fit example for Lhcb1 wild type at 680 nm excitation wavelength, fluence dependence.
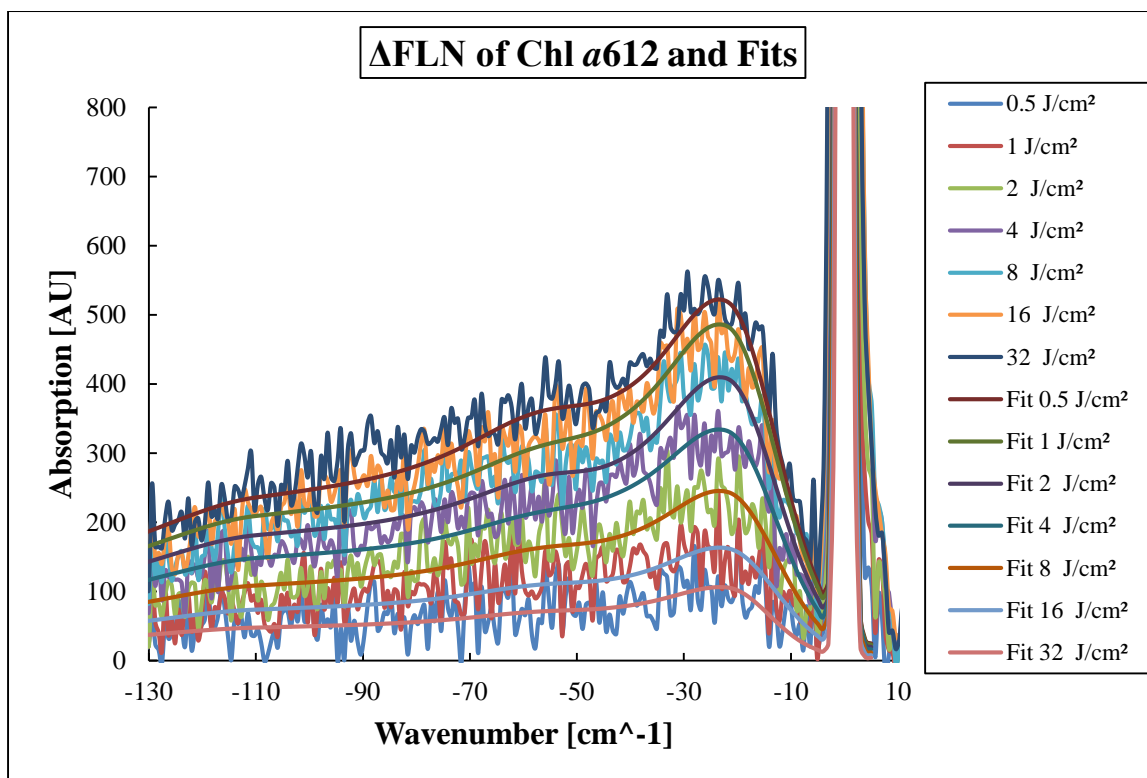
Figure 10: ΔFLN spectra fit example for Chl *a*612 mutant at 680 nm excitation wavelength, fluence dependence.


Figure 11: ΔFLN spectra fit example for Chl *a*610 mutant at 678 nm excitation wavelength, fluence dependence.

The phonon – wings of the ΔFLN spectra of all LHC II samples show a pronounced peak around ~18 cm^-1, a shoulder near ~65 cm^-1, and a further peak at ~110 cm^-1. A similar broad and asymmetric profile have been seen for other ΔFLN experiments on native LHC II from spinach, WSCP (Pieper, et al., 2011), LH2 or LH1. The parameters obtained for these examples can be seen in Appendix 1.

The S – factors obtained generally depend on fluence and increase with increasing fluence due to the saturation of the resonantly excited spectral features, see above. Therefore, the more reliable S-factor according to literature (see Chapter 2.1.2) is that one fitted for the lowest fluence for the selective excitation laser wavelength.

The data reveals a slight decrease of S – factor with increasing excitation wavelength to the red side of the IDF for Lhcb1 wild type sample. This indicates that the non – resonant contribution to the delta FLN spectra at the blue side of the IDF is larger than at the red side and may also point to an additional influence of EET from higher energy states at the blue side of the IDF.
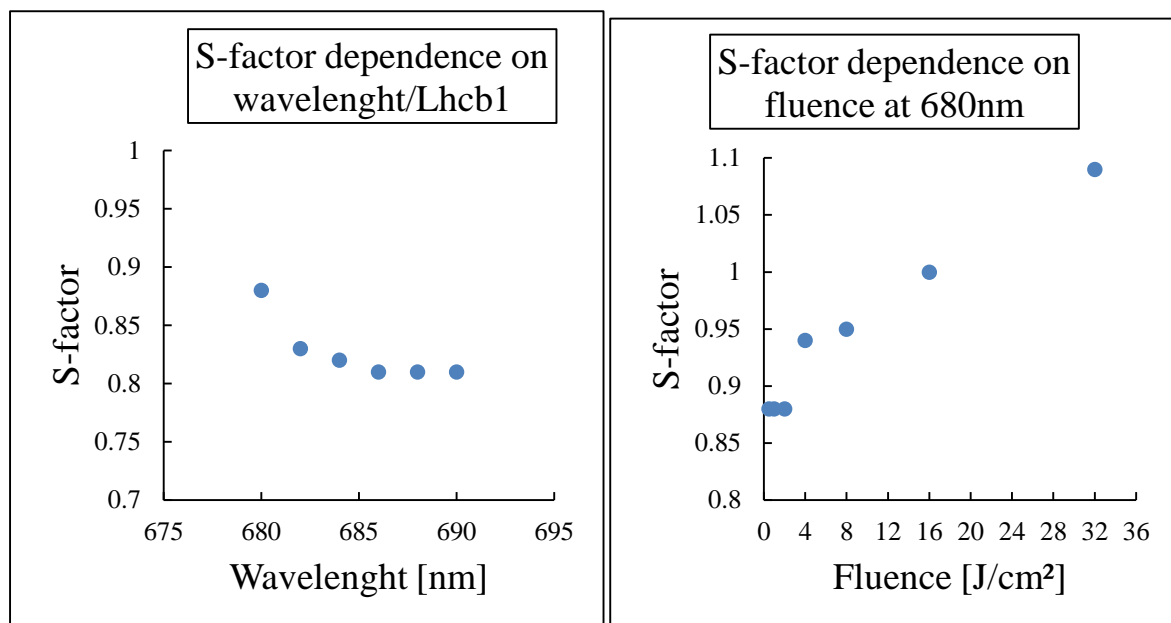
Figure 12: S-factors fitted for monomeric Lhcb1 at different excitation wavelengths (left) and S-factors fitted for Lhcb1 at the excited wavelength of 680 nm with different fluences (right).

From Figure 12 (left) it is clearly seen that with the increasing the wavelength the S-factors fitted for wild type LHC II decreases slightly from ~0.9 to ~0.8. There is a bigger decrease if we compare the   S – factors obtained at different fluences for a specific excitation wavelength as shown in Figure 12 (right). In this case for Lhcb1 complex can decrease from 1.1 at high fluence rate to ~0.88 in the low fluence range.

The behaviour seen for Chl a612 and Chl a610 mutant samples are similar regarding the fluence dependence within the one excitation wavelength. Differences appear from fitting the S-factors for different excitation wavelengths in low – fluence range (Figure 13). Removal of one Chl affects the excitonic coupling in a different way for our mutant samples.
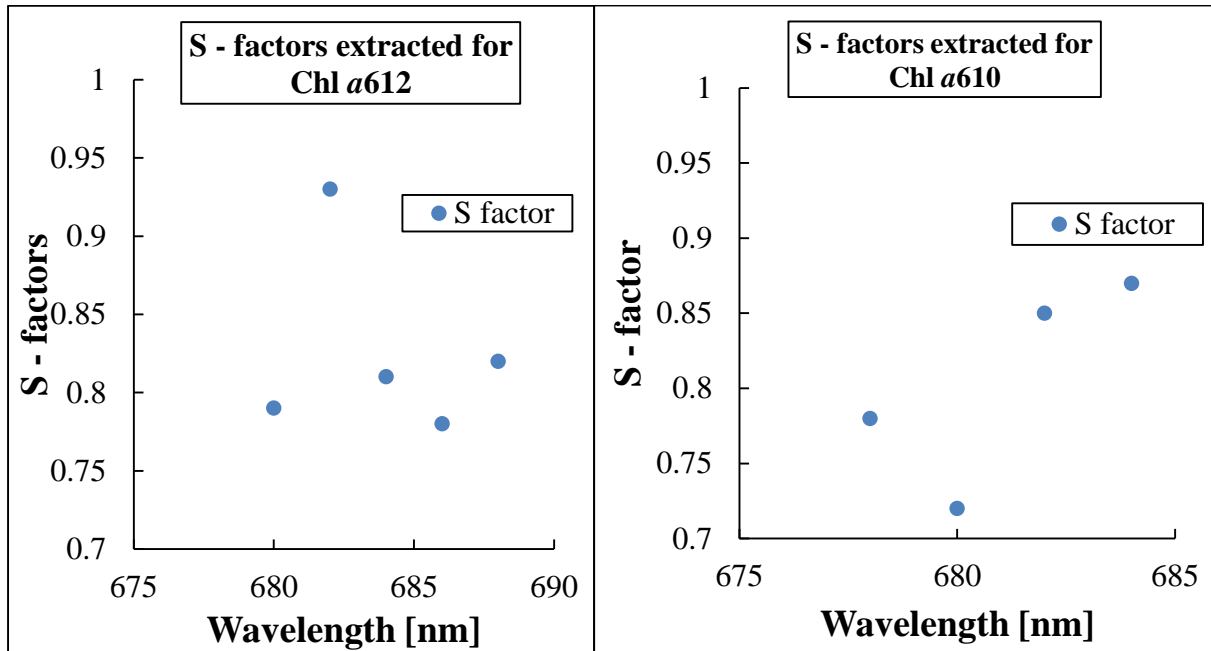

Figure 13: S-factors fitted for Chl *a*612 (left) and for Chl *a*610 excitation wavelength dependence in the low – fluence range (0.25 mJ/cm²).

3.3   CD spectra of LHC II samples

The LHC II wild type shows a non – conservative spectrum in CD measurements as seen in Figure 14. The negative ~650 nm peak is considered to be caused by the Chl b activity, while the positive ~660 nm, ~670 nm and negative ~680 nm is due to the Chl a activity. Chl b peak is related to the intrinsic structure of it (helical structure). The positive ~660 nm, ~670 nm and the negative ~680 nm peaks are linked to the excitonic coupling in the pigment molecule

caused by the light excitation (Müh, et al., 2010).
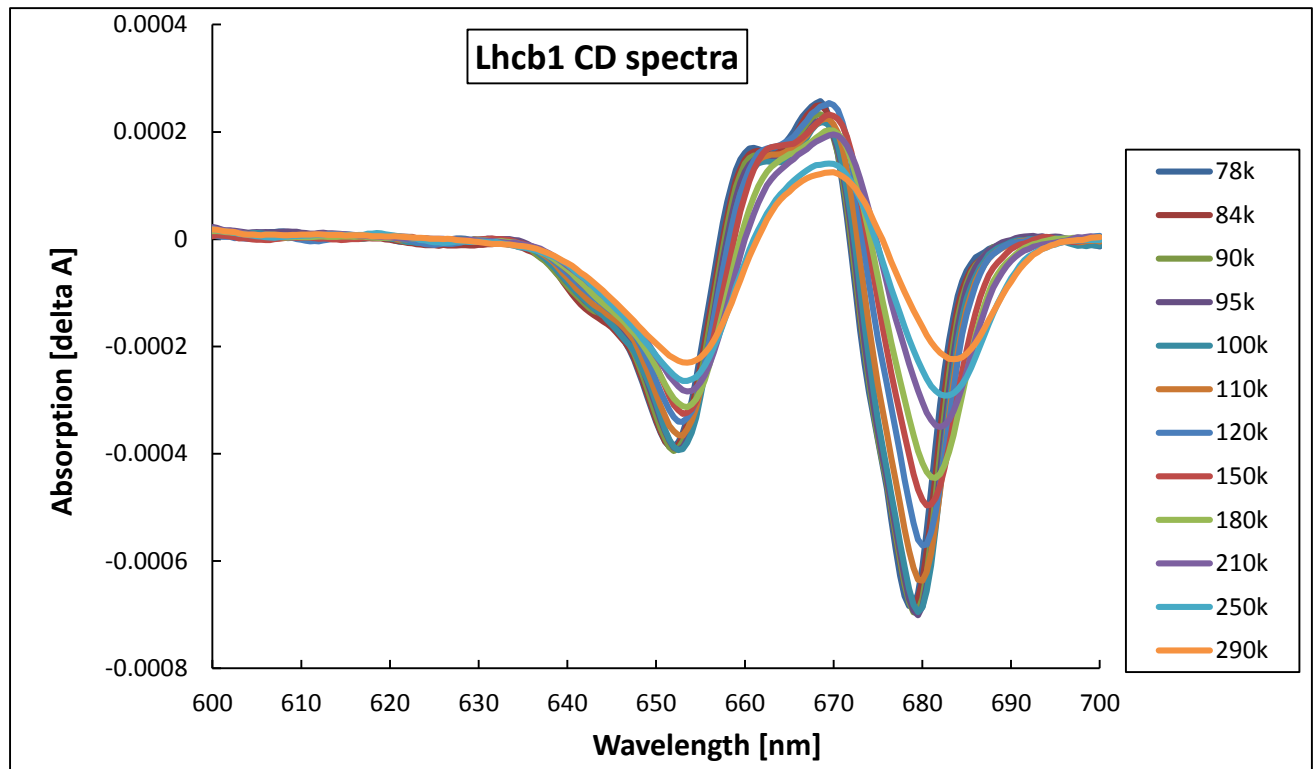
**Figure 14:** CD spectra of the intact Lhcb1 in the 78K – 290K temperature range.

I have fitted the peaks with Gaussian shape band for a better evaluation of the spectra. From the Lhcb1 CD spectra it can be seen that with increasing the temperature the four peaks shift towards the red and also a change in the intensity of the peaks occurs. Basically, all four peaks suffer from a decrease in its intensity with the increase of temperature.

From Figure 15 we can distinguish the following aspects: a) the ~650 nm peak shifts from 651 nm at 78 K to 653 nm at 180 K and after we can see a plateau until 290 K around 653 nm; b) the ~660 nm peak has a steep shift from 660 nm at 78K to 666 nm at 290 K; c) the ~670 nm peak seems to have the same behaviour as ~660 nm peak with a smaller shift from 669 nm at 78 K to 669 nm around 180 K and after stabilizing around 669 nm until 290 K; d) the ~680 nm peak has a gradual peak shift from 678 nm at 78 K to 683 nm at 290 K. The fitted spectral uncertainty for Lhcb1 is ±0.35 nm.
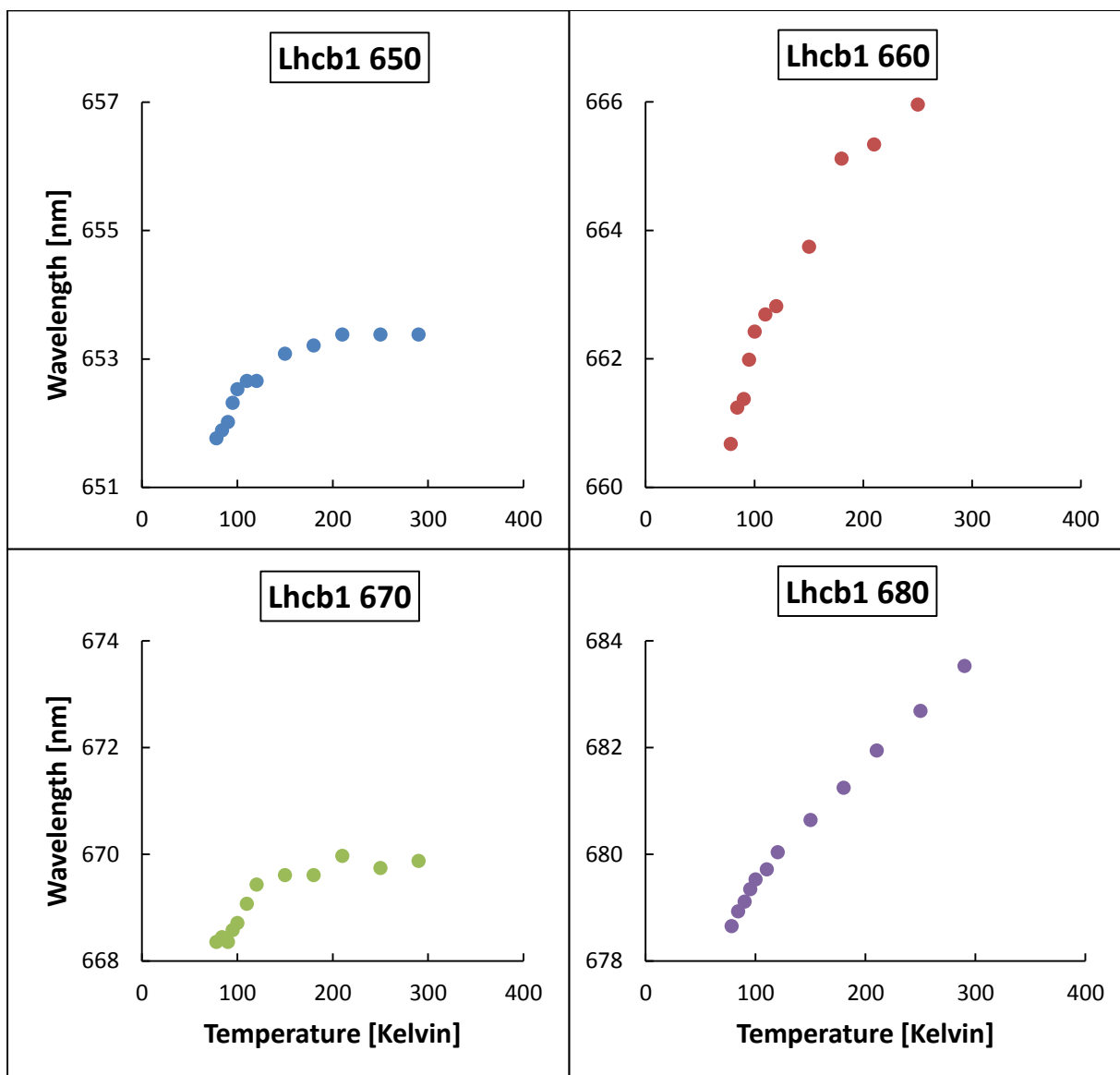
Figure 15: CD peaks shift with temperature for intact Lhcb1

The fitted Gaussian band with the peaks shows an increase of fwhm with the increase of temperature as seen from Figure 16: ~650 nm peak raises from ~200 to ~290 cm^{-1}, 660 nm peak raises from ~115 to ~180 cm^{-1}, ~670 nm peak increases from ~115 to ~160 cm^{-1} and the ~680 nm peak raises from ~140 to ~220 cm^{-1}.
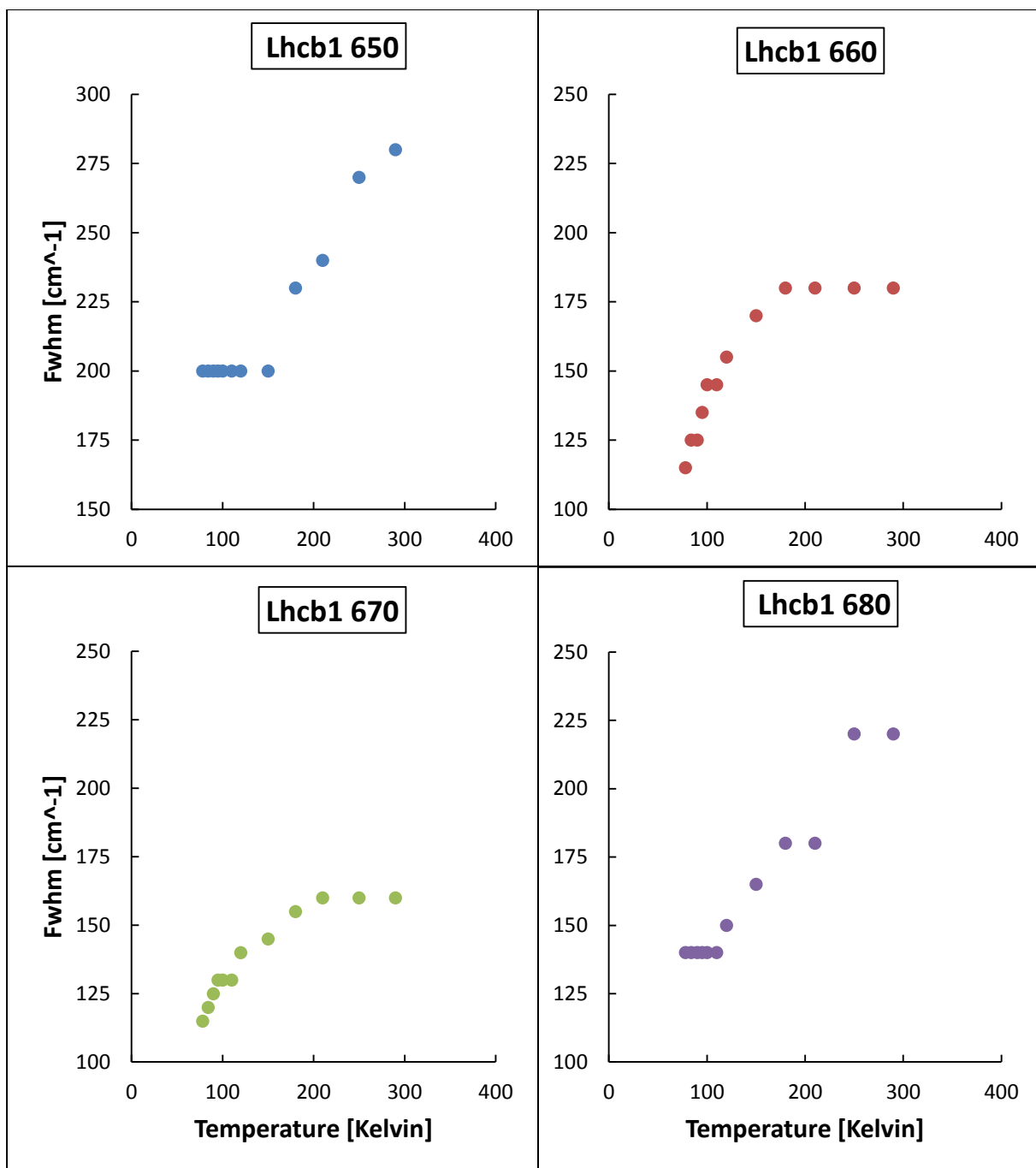
Figure 16: Fwnm shift with temperature for Lhcb1

In the CD spectrum of Chl a610 the removal of one Chl is clearly seen in the change of the spectrum shape: the overall intensity of the positive peaks are smaller and a higher change is seen for the positive ~670 nm peak where its intensity is very low compared with the CD spectrum of Lhcb1. The Chl a610 mutant shows the same characteristics with the increase of temperature: the peaks shift towards red region and their intensity decreases as seen from

Figure 17.
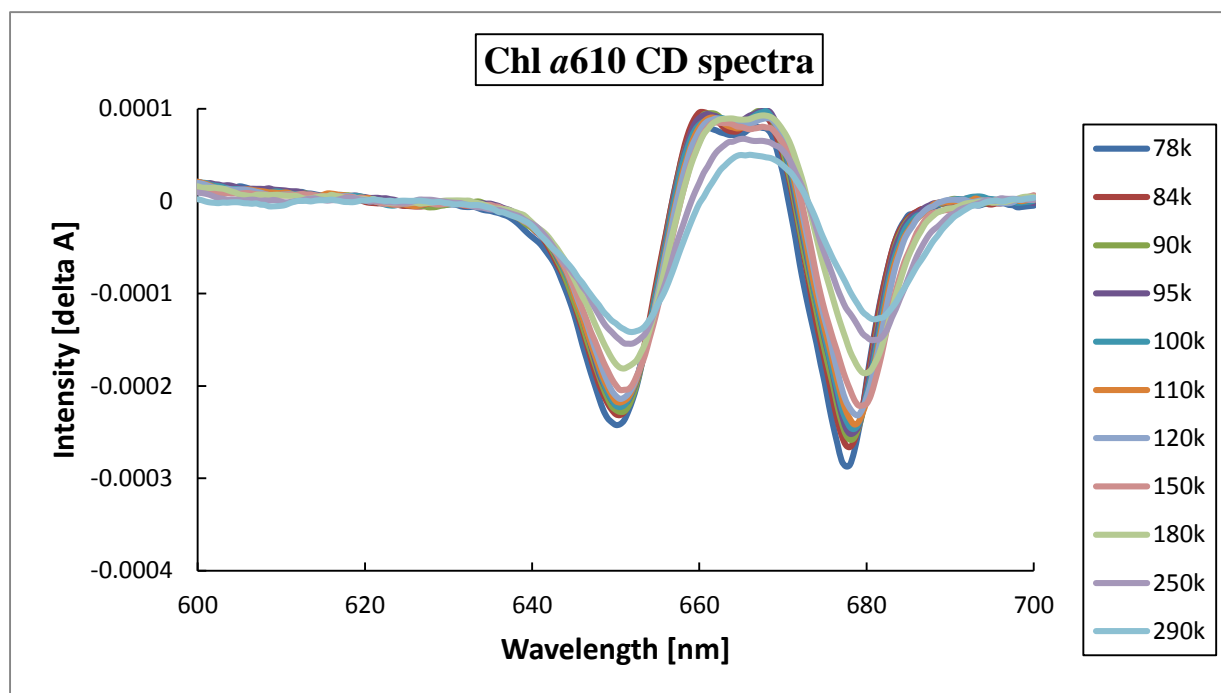
Figure 17: CD spectra of the a610 mutant in the 78 K – 290 K temperature range.

From Figure 18 we can distinguish the following aspects: a) the ~650 nm peak linked to Chl b shows a red shift from ~650 at 78 K to ~652 nm at 290K; b) the ~660 nm peak shifts from ~660 nm at 78K to ~664 nm at 290K; c) the ~670 nm peak shows a slight change of just one nm shift to red from ~667 nm at 78 k to ~668 nm at 290 K; d) the ~680 nm peak shifts from ~677 nm at 78 K to ~681 nm at 290 K. The uncertainty of the fitted spectra for Chl a610 mutant is ±0.45 nm
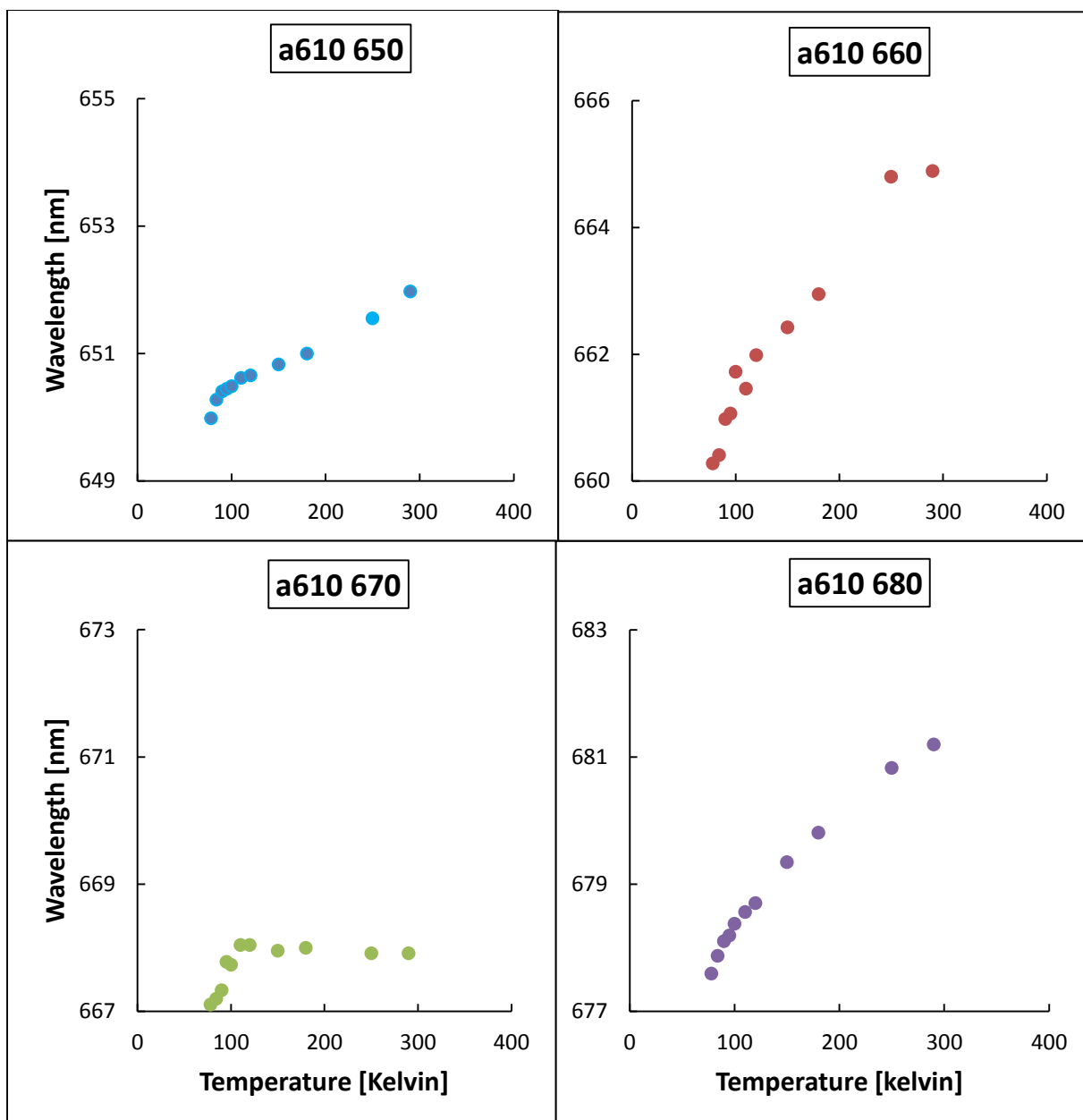
Figure 18: CD peaks shift with temperature for a610 mutant

The fwhm for Chl a610 mutant of the four peaks broadens with the increase in temperature, as following: the ~650 nm peak increases from ~200 to ~260 cm^{-1}, ~660 nm peak increases from ~110 to ~194 cm^{-1}, ~670 nm peak broadens from ~110 to ~166 cm^{-1} and ~680 nm peak increases from ~140 to ~215 cm^{-1} (Figure 19).
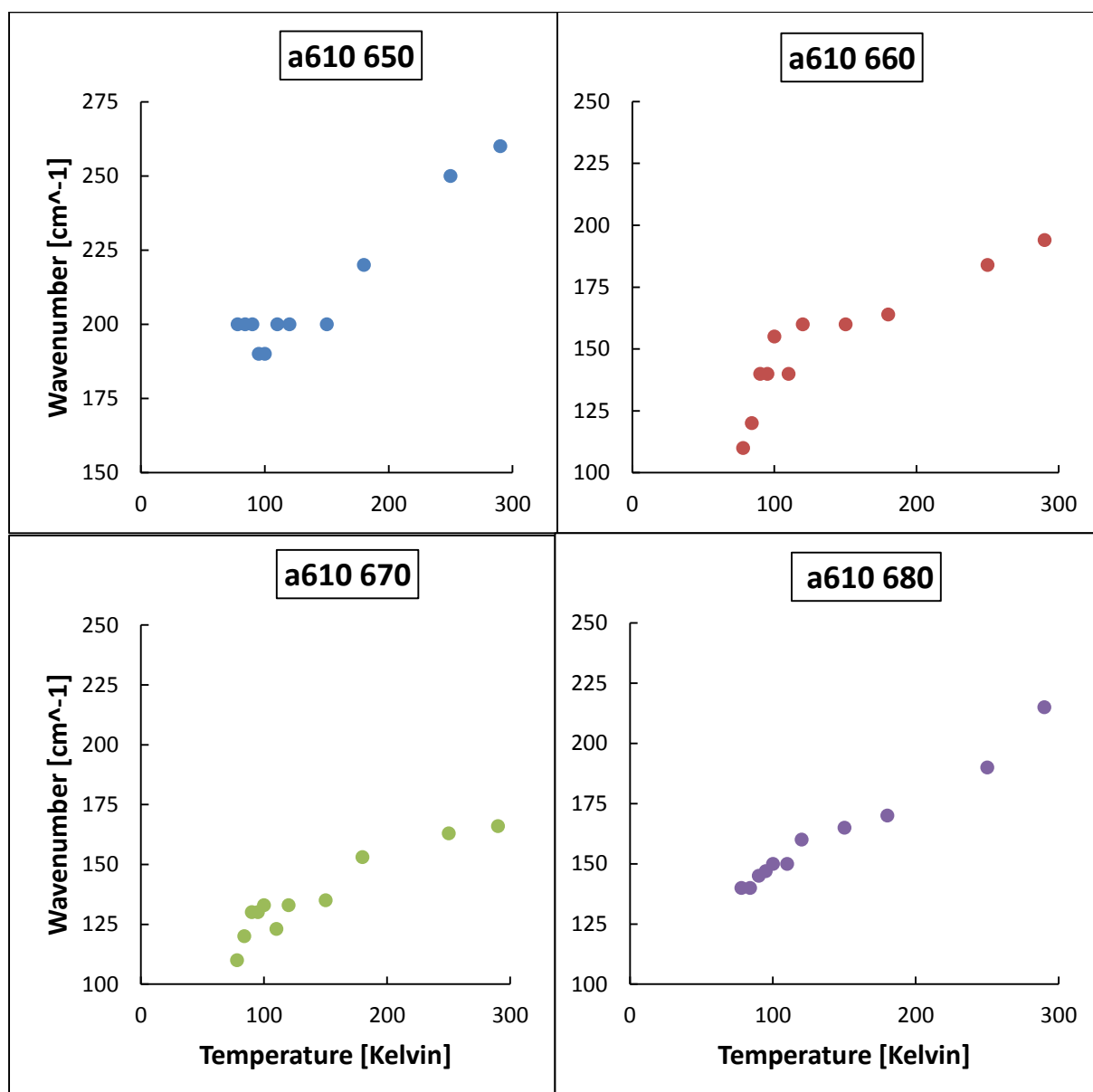
Figure 19: Fwhm shift with temperature for a610 mutant

The CD spectra of Chl a612 mutant display a change in its shape and intensity caused by the removal of one Chl. When comparing with the intact Lhcb1 CD spectra, we could see that the ~670 nm peak is missing (a broadening of the two peaks, no longer distinguishble one from another) and the ~660 nm peak lowered its intensity. The Chl a612 mutant spectra displays the same trend with the increase of temperature: spectral shifts of the peaks towards the red region and intensity decrease of the peaks. The fitted spectra uncertainty for Chl a610 mutant is ±0.32 nm. (Figure 20).
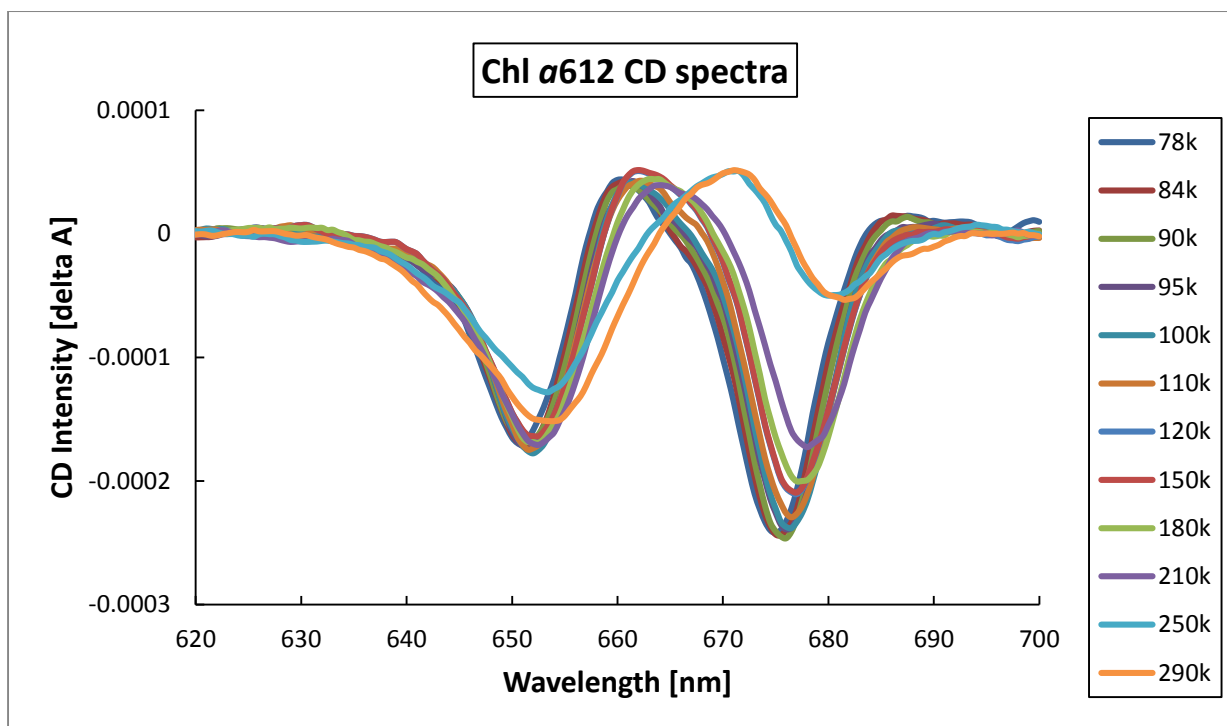
Figure 20: CD spectra of the a612 mutant in the 78K – 290K temperature range.

From Figure 21 we can see how the spectral peaks shifts with the increase in temperature: ~650 nm peak shifts from 650 to 653 nm, ~660 nm peak shifts from 660 to 670 nm and the ~680 nm peak shifts from 674 to 681 nm. We can see that at 250 K and 295 K temperature point there is a sudden increase of the ~680 nm peak towards the red region of the spectrum which means that our complex it might suffer a structural change with the trasitions to higher temperature (above 180 K).
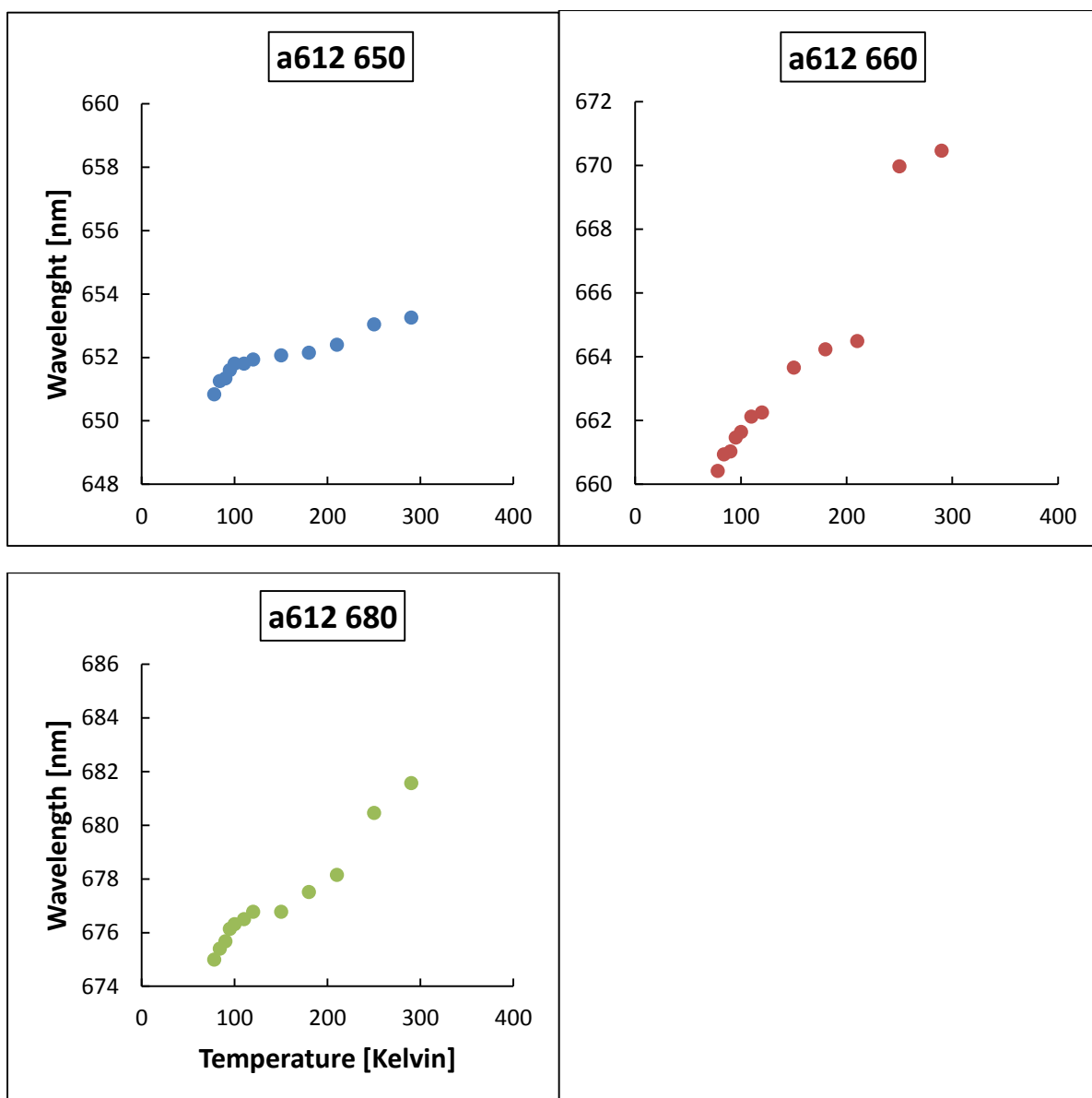
Figure 21: CD peaks shift with temperature for Chl *a*612 mutant

The fwhm widens with the increase in temperature for the Chl *a*612 mutant as seen from Figure 22: ~650 nm peak rises from 190 to 320 cm^{-1}, ~660 nm peak rises from ~115 to ~200 cm^{-1} and the ~680 nm peak has slight variations from ~180 to ~190 cm^{-1} and back to ~170 cm^{-1}. The spectra of the 3 samples can be split into three temperature regions: from 75 K to 120 K where there is a constant slowly shift to the red region, from 120 K to 210 K it seems there is a plateau (or a flat region where the peak shift is very small) and a third region between 210 K to 290 K where there is a rapid increase towards the red region of the spectra.
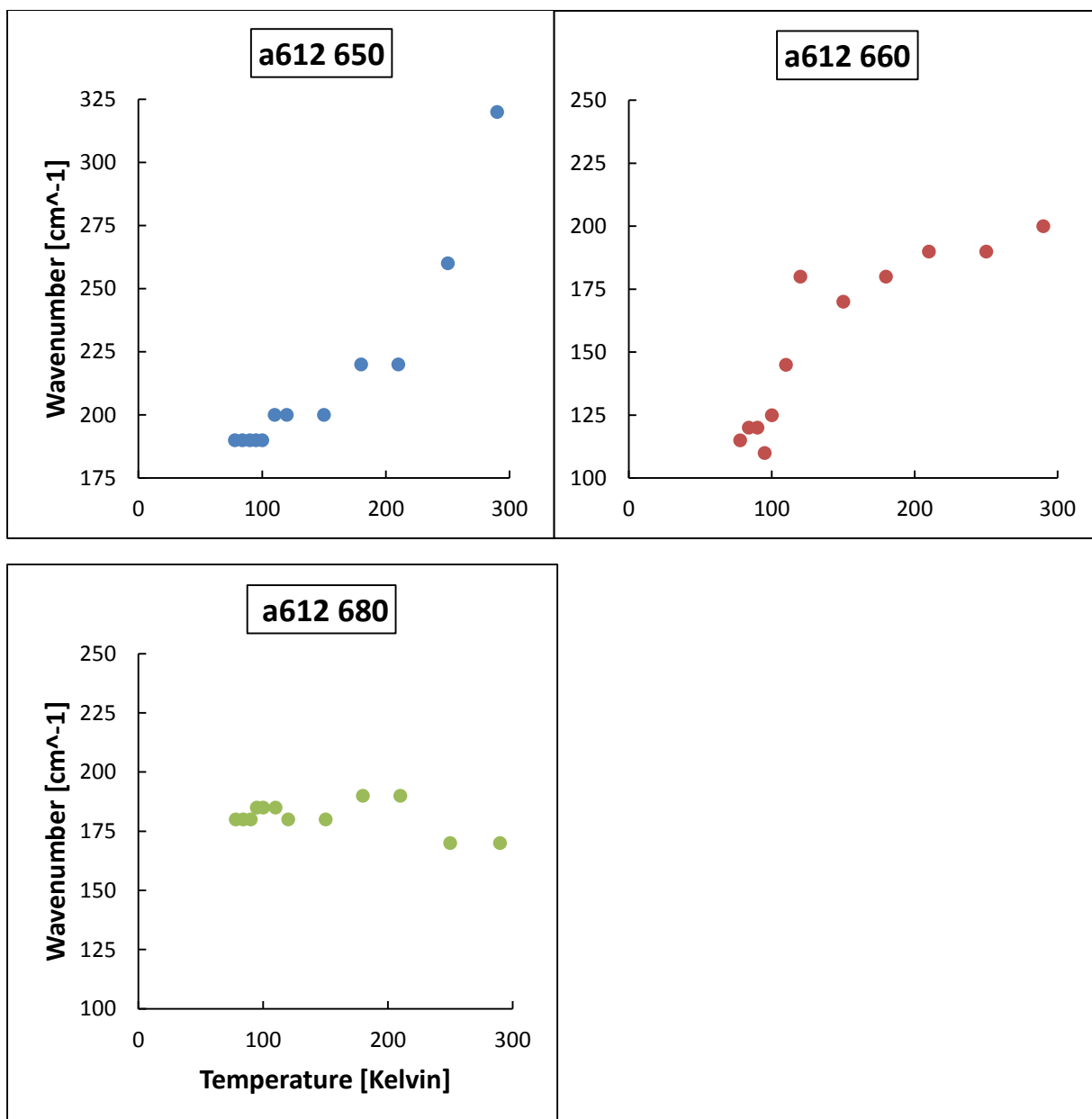
Figure 22: Fwhm shift with temperature of Chl *a*612 mutant peaks

The peaks from all the CD spectra for all the 3 samples shows, beside a shift towards longer wavelenghts, also an intensity change with the increase of temperature. In the figure 23 and 24 we can clearly destinguish a drop in intensity during transition to higher temperatures for the ~650 and ~680 peaks. The intensity spectra were plotted afte normalization to the ~650 nm peak considered not to interfere to the excitonic pair (~660 nm/670 nm and 680 nm) in the CD spectra.
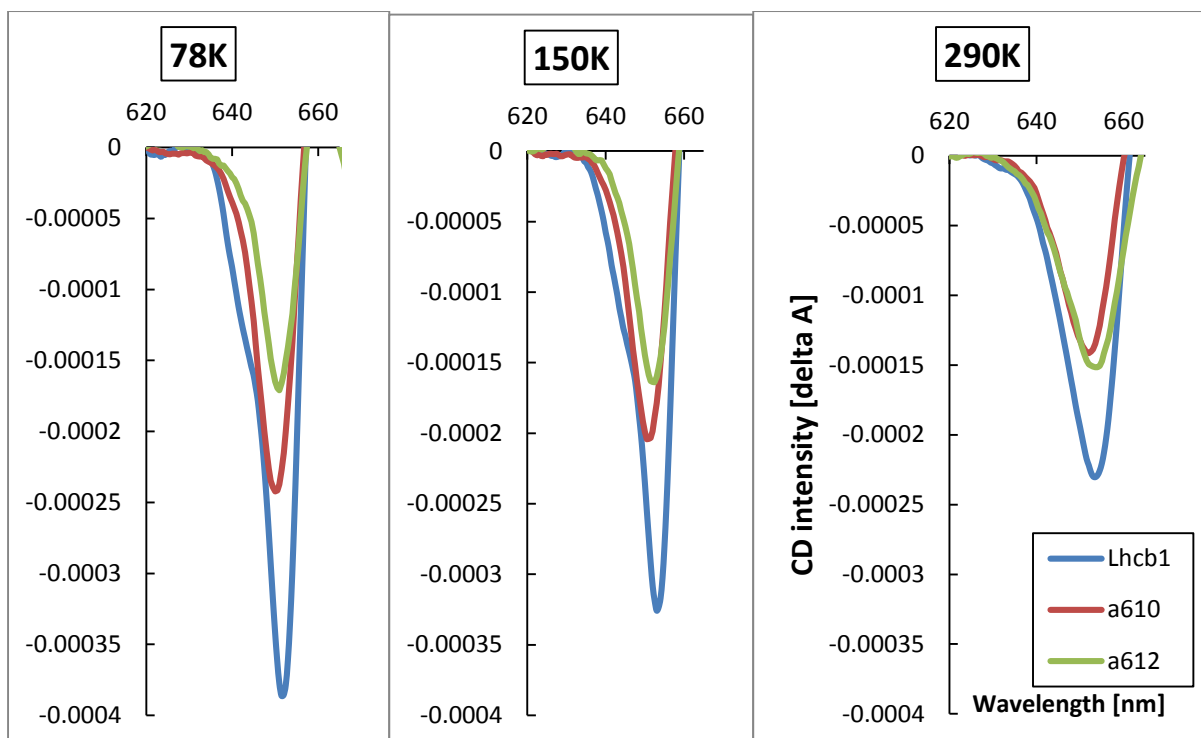
Figure 23: CD intensity of the ~650 peak within 3 different temperatures 78K, 150K and 290K.
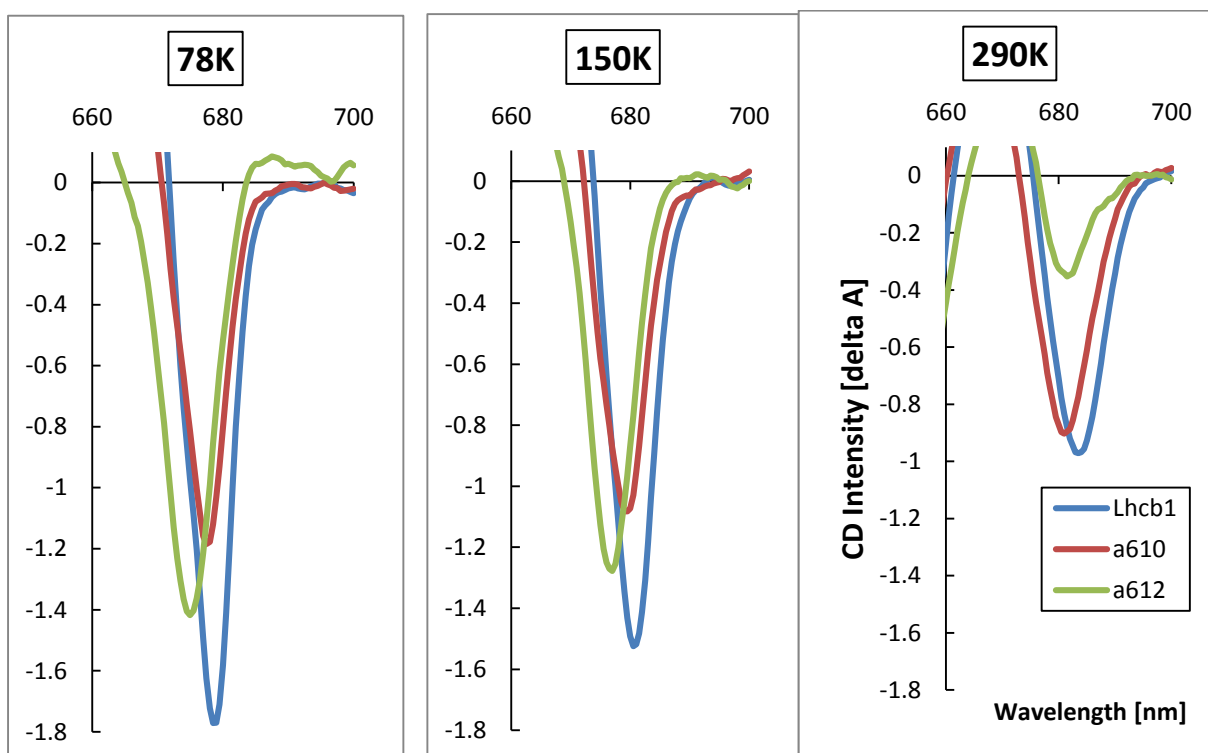
Figure 24: CD intensity of the ~680 peak within 3 different temperatures 78K, 150K and 290K.

In the Figure 25 it is interesting to observe that the ~680 peak of the two mutant samples is blue shifted comparing to the intact Lhcb1 peak in the given temperature range. With temperature increase we can observe a broadening of the spectra and also a lowering in intensity (Figure 18). This suggest that both Chl *a*610 and Chl *a*612 contributes to the low-

energy states of LHC II. Chl *a*612 blue shift is more pronounced with decreasing temperature and it is ambitious to say that this Chl is the energetically lowest electronic state at cryogenic temperatures.
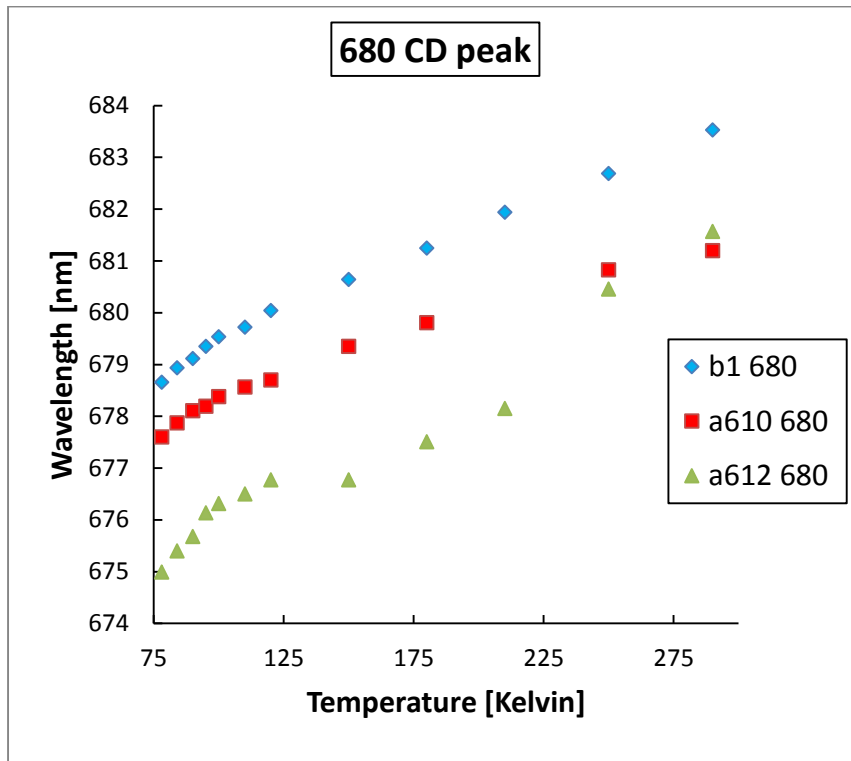
Figure 25: CD, temperature dependence of the ~680 nm peak (±0.35 nm)

For the positive peaks of the CD spectra the changes are more intense and significant (Figure 26). When comparing to Lhcb1 CD spectrum the Chl a610 suffers a decrease in intensity for both ~660 and ~670 nm peaks. With increasing the temperature the ~670 nm peak lowers its intensity and at 290 K the peak can not be well distinguished anymore. The Chl a612 mutant has more intense changes in its CD spectra. At a first glance, at 78 K, the ~670 nm peak is completely missing and the remaining ~660 nm peak is very low in intensity compared with the Lhcb1 ~660 nm peak. The big change comes with aproaching room temperature when we can see a sudden shift in its peak position towards red. Chl a612 is a central Chl of the intact LHC II in the terminal emitting cluster formed by a610 – a612 – a611, which means when removing it it affects more the total excitonic contribution in the spectra.

In summary, upon removal of Chl *a*610 from Lhcb1, which is considered to be situated at the one extremity of the Chl trimer, excitonic coupling should be still present in the remaining Chl dimer. Furthermore, if the central Chl *a*612 of the Chl trimer is removed from the complex the lowest excited stated should be rather localized. Therefore, the excitonic coupling within the

cluster formed by Chl $a610 - a612 - a611$ should be affected differently in the mutants studied within this work. This may explain the different spectral positions of the ~680 nm band shown in Figures 24 and 25. However, further excitonic calculations are required to verify this interpretation.
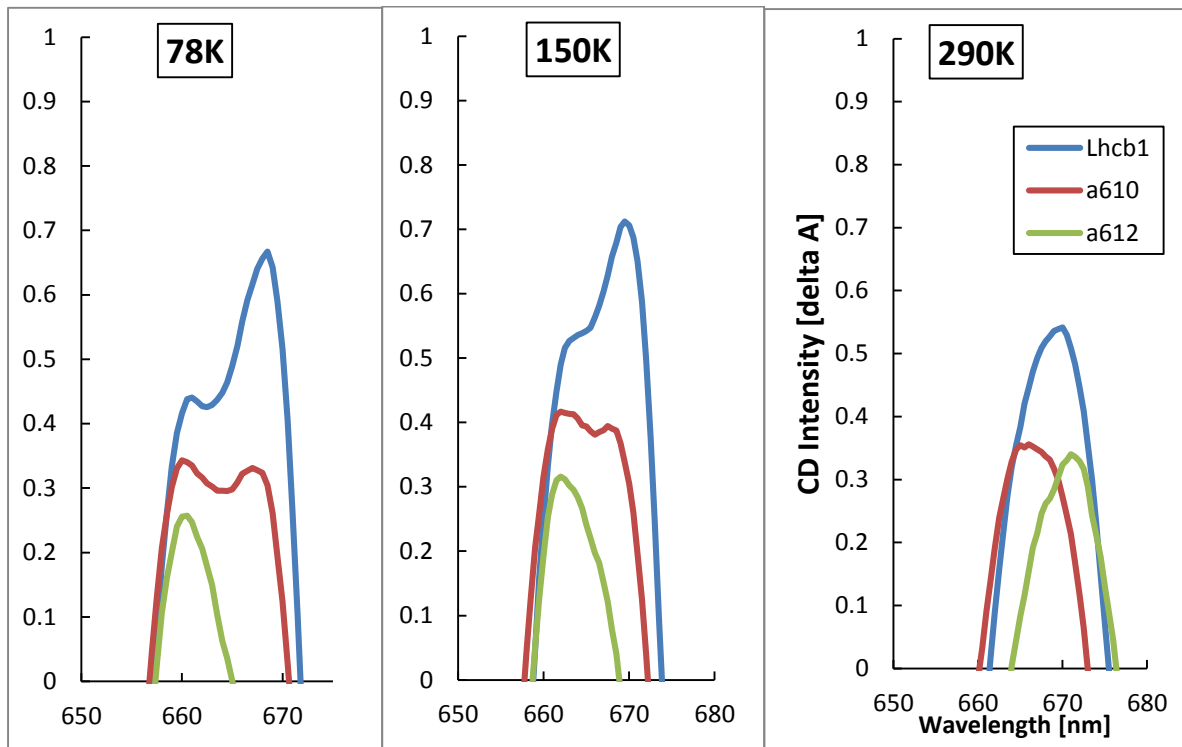
Figure 26: CD intensity of the ~660 and ~670 peak within 3 different temperatures 78K, 150K and 290K.

4. Discussion

4.1. Comparison of ΔFLN with other selective spectroscopic techniques

The ΔFLN technique has been used in the present thesis to provide insights into electron – phonon coupling of Chls in monomeric Lhcb1 and two other mutant samples, Chl a610 and Chl a612. Also it has been compared with other techniques from the point of view of the accuracy of the information in extracting the S – factor values for our pigment - protein complex. It is relevant to say that also the electron – vibrational interactions can be determined with this technique (not shown in this thesis).

The results clearly exhibit many advantages in using this technique in calculating electron – phonon and electron – vibrational coupling strengths. But, it can be used in connection with complementary techniques as SHB, CD or QENS to further determine the excited states positions and protein dynamics of the pigment – protein complex.

Based on our simulations, in SHB experiments the shape of the pseudo-PSB strongly depends on the inhomogeneous width as seen in Chapter 3.1.1., therefore much attention is needed when calculating S – factors from SHB data. Even when the inhomogeneous width is larger than the width of the PSB the shape of the pseudo – PSB never reflects the true shape of the real – PSB. The reason for this effect lies in the nature of the pseudo-PSB, which is comprised of electronic lines which absorb the burn laser light via their PSBs coincident with the burn frequency. Outside of the IDF, these electronic lines are not present, so that the pseudo-PSB is artificially cut off by the IDF.

We have also shown that the electron – phonon coupling strengths values based on ΔFLN data were closer to the real value compared with SHB results obtained when taking into account the real- and pseudo-PSB features which were significantly off from the true value of 1. Again, this is the result of technical limitations of the SHB technique, where the pseudo-PSB is suppressed by the shape of the IDF depending on the IDF width leading to an underestimation of S, while the real-PSB contains contributions from the multi-PSB leading to an overestimation of S.

Furthermore, we have demonstrated that the apparent Huang – Rhys factor deduced from ΔFLN data depends not only on the excitation within the IDF but also on fluence and position of the excitation frequency within the IDF due to the fluence-dependent saturation of resonant contributions and the varying non-resonant contribution. In case we increase fluence to get

more intense spectra we also increase the non – resonant contribution to the spectra, therefore the S – factors fitted are overestimated.

With our research we have brought new data for improving the extraction of the S – factors with these two selective techniques, and showed that ΔFLN technique could be more reliable in case of taking extra care about the fluence dependence and the position of the excitation wavelength within the IDF.

4.2   Electron – phonon coupling of excitonic states of LHC II

As reported in the literature (Rogl, et al., 2002) the terminal excitonic state of LHC II is reported to be situated at Chl a612 at room temperature. This seems to be in line with other studies which reported (Grondelle & Novoderezhkin, 2005) the lowest excitonic state of LHC II on a cluster with strongly coupled Chl molecules a610 – a611 – a612. At cryogenic temperatures (4.5K) SHB studies (Pieper, et al., 2009) concluded that the lowest excitonic energy level for monomeric LHC II is situated at ~680 nm on a single Chl molecule having an S-factor of 0.9 and a strong asymmetric one – phonon shape.

Our results, using ΔFLN technique to calculate the S – factors, are in agreement with the previous studies for the native LHC II. For the Lhcb1 wild type, according to ΔFLN spectrum in the low – fluence range (at 680nm excitation wavelength), the electron – phonon coupling strength of the lowest excitonic energy pigment is 0.88. As seen in Chapter 2.3 the S – factor calculated for Lhcb1 shows a decrease with increasing excitation wavelength and also an increase with increasing the burn fluence within the same excitation wavelength.

For the Chl a610 and Chl a612 mutants the S – factors calculated for different excitation wavelengths shows an irregular pattern and lower values. The S – factors fitted with fluence dependence follow the same trend: increasing the burn fluence the S – factors fitted increase as well. For example, in case of Chl a612 mutant the S – factor fitted at 680 nm excitation wavelength in the low – fluence range is 0.79 and for Chl a610 mutant the S – factor fitted at the same excitation wavelength is lower than previous one at 0.72.

In summary, the S-factors obtained for LHC II and their wavelength dependence are only slightly affected by mutation at 4.2 K. A possible interpretation is that the wavelength dependence of S in wild type LHC II is due to a complex superposition of –factors from different low-energy states, while the spectral position of Chl a612 is blue-shifted so much at 4.2 K that changes upon mutation are visible only at the blue side of the fluorescence band. Therefore, the S-factors observed at 680 nm and longer wavelengths are mainly characterized

by another Chl, e.g. a Chl carrying a widely localized low-energy state like Chl a604 as proposed by Pieper et al. (2009).

4.3   Temperature dependence of excited state positions of LHC II

The temperature dependence of the absorption spectrum of LHC II pigment – protein complex ishould be mainly determined by the coupling of the electronic transition to phonons and low frequency intramolecular vibrations.

The mutations cause a clear change in the absorption spectra in certain spectral regions. That's why through subtraction of the absorption spectrum of LHC II lacking one Chl from the absorption spectrum of intact LHC II we can determine the difference spectrum which can be assigned to the missing Chl. For example, when comparing Lhcb1 and Chl a612 spectra, the difference spectra exhibit a major peak in the vicinity of 677 - 680 nm, negative intensities at ~653 and ~666 nm as well as further minor absorption changes throughout the entire-spectral range. The major effect upon mutation of Chl a612 is the loss of absorption intensity in the vicinity of 677 - 680 nm, which can be attributed mainly to the absorption of Chl a612.

The absorption difference spectra of the mutant samples have a dependence on temperature. In the temperature range of 75 K and 290 K both mutants shift their absorption difference spectra peaks towards higher wavelengths by ~7 nm. (Figure 27). The temperature dependence of the Gaussian peak fits is not linear across the whole temperature range as expected. We can distinguish two temperature regions: one from 75 K until ~240 K where the shift behaves close to linear dependence and one region from 240 K to 290 K where we can observe a sudden shift of the peak towards red region of the spectrum. . Identifying the exact temperature where the shift is more pronounced needs to select closer temperature spacing when doing the future experiments in the 180 K - 290 K.
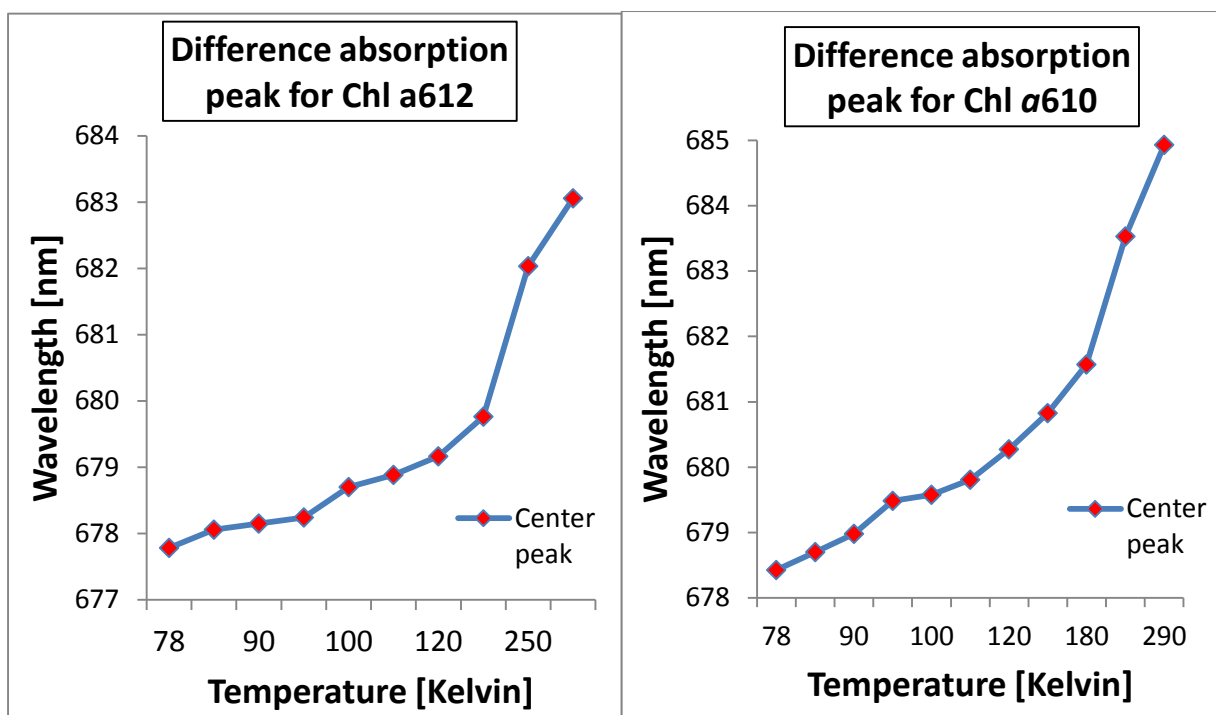
Figure 27: Temperature dependence of the difference absorption peak fitted with a Gaussian shape band of Chl *a*612 (left) and Chl *a*610 (right) mutants (±0.35 nm)

Also, the same behaviour is observed for the widths (FWHM) of the Chl a610 and Chl a612 fitted with a Gaussian shape as observed in Figure 28. After ~240 K there is a sudden increase in width for both mutants. These find only add to our understanding that in this temperature range there is an electronic transition and a change in conformation of the complex which influences the energy sites of individual pigments.

45
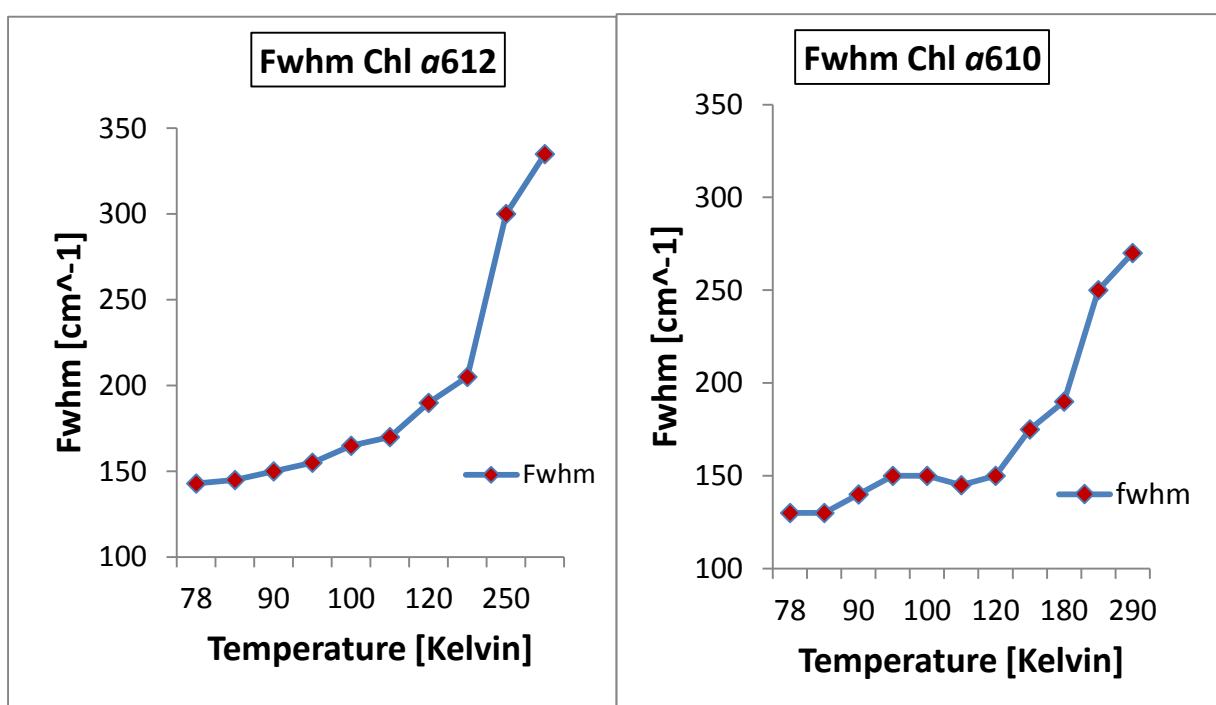
Figure 28: Dependence of the fwhm fitted with a Gaussian shape band within the temperature range of 75 K and 290 K for Chl *a*610 (left) and Chl *a*612 (right) mutants (±0.4cm^-1)

These results resemble the temperature-dependent shifts of the CD bands presented above and may help us to build a potential model for our pigment – protein complex in different temperature ranges. The temperature dependence of the system can be described by an asymmetric double well potential, where these V1 and V2 wells describes two energetically inequivalent protein conformations.

Having in mind this description illustrated in Figure 29, the system can have a V1 conformation at low temperatures and a different V2 conformation at an elevated temperature. The probability to find the system in higher –energy conformation increases with increasing temperature (Vrandecic, et al., 2014).

In the first conformation V1, the electronic ground state potential of V1 is lower in energy than the one of V2. With the increasing temperature, V2 ground state is thermally populated. Thus, the transition energy of an electronic excitation from ground state E0 to the excited state E1 is smaller in conformation V2 than in V1. At low temperature there is a single higher-energy transition $\Delta E1$, while at elevated temperatures a second $\Delta E2$ lower-energy transition will accompany the $\Delta E1$ transition in absorption.
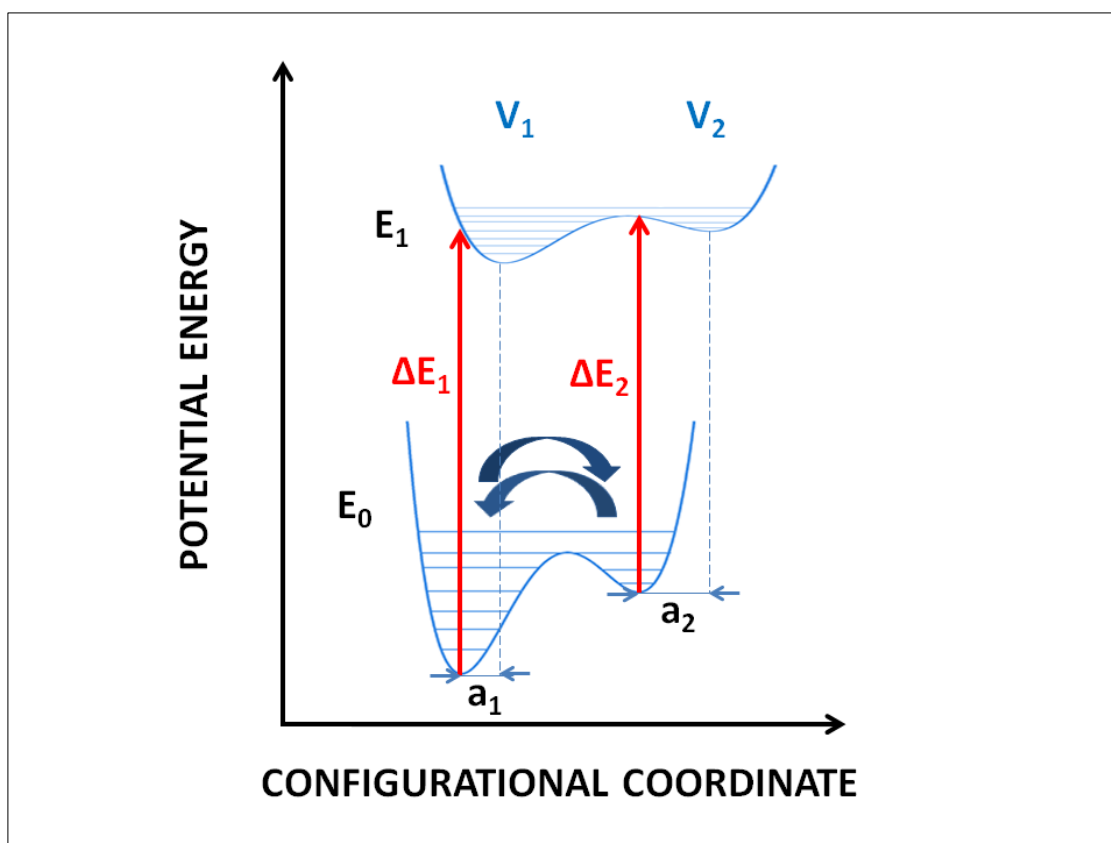
Figure 29: Schematic potential energy diagram of a pigment embedded into an amorphous protein matrix assuming two different protein conformations V_1 and V_2 represented by asymmetric two level systems in both, the ground (E_0) and the excited electronic state (E_1) of the pigment molecule, respectively. The displacements between the equilibrium positions of conformations V_1 and V_2 are labelled by a_1 and a_2, respectively. The two energetically inequivalent optical transitions resulting from the potential energy diagram are shown by red arrows and labelled by ΔE_1 and ΔE_2, respectively. Bold arrows indicate thermally-activated conformational motions between protein conformations V_1 and V_2, [*Permission granted*]

An interesting aspect is the blue shift of the ~680 nm peak in Chl a612 CD spectra in the 75 K – 290 K range. This result is in agreement with the absorption difference spectra result, which also shows a blue shift of the Chl a612 absorption peak.

We can also observe in Figure 25 that after 180 K the CD spectrum of Chl a612 mutant exhibits a sudden shift towards the red region. This implies that the LHC II may have a different conformation and it might be affected by the protein environment. A structural transition may possibly occur at ~77 K and at ~240 K as well.

These results can provide insights into protein environment of Chl a612 and conclude that it might form bi- or even tri – stable conformations, which leads to a strong temperature

dependence of Chl site energies (one at low temperature and another conformation starting with a determined higher point on the temperature scale).
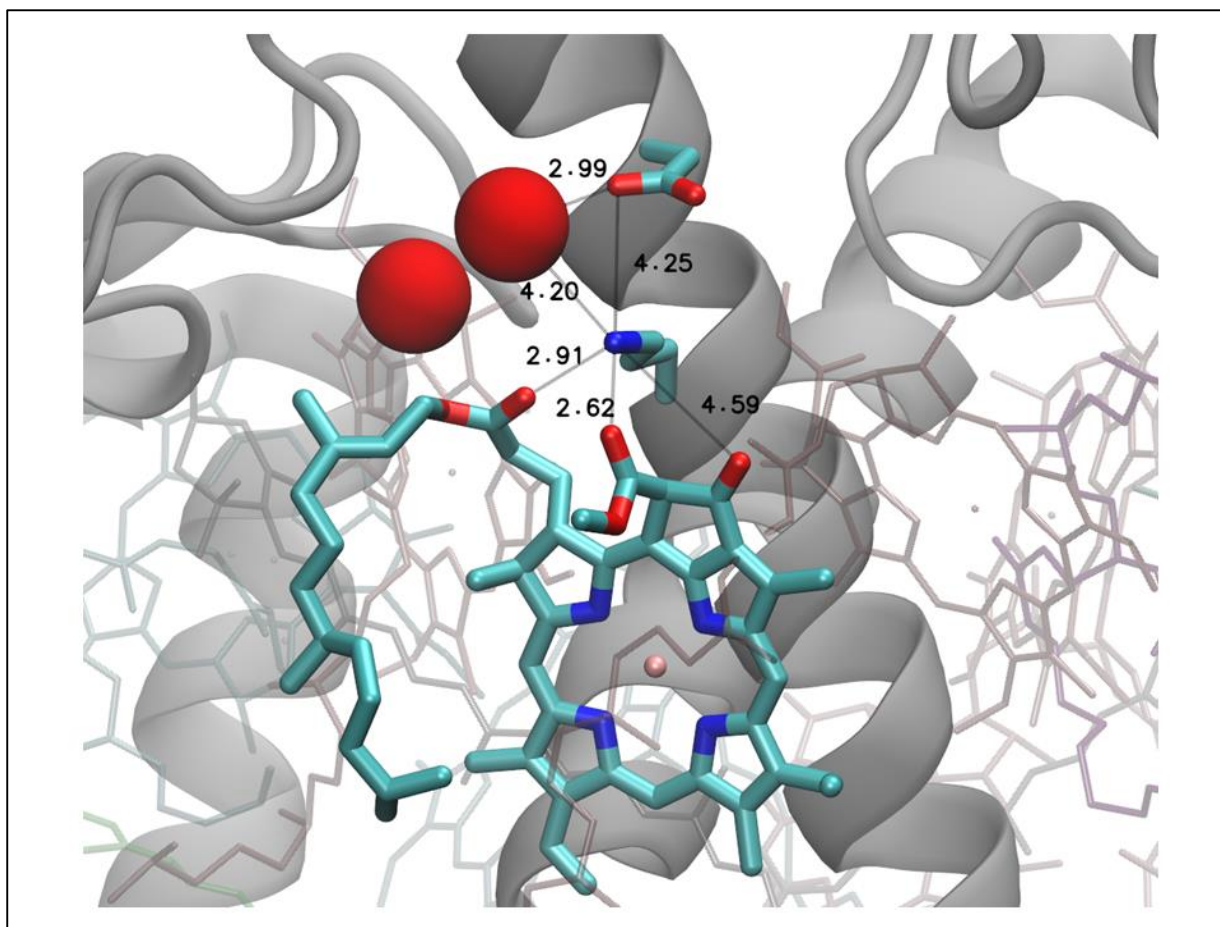
Figure 30: Protein environment of Chl 2/Chl*a* 612 according to the LHC II structure of Standfuss et al. (protein data bank code: 2BHW). The charged Lys 179 residue may form hydrogen bonds especially with ester groups of the phytyl chain or ring E of Chl 2/Chl*a* 612, but also with another Chl sidechain as well as with a Glu residue and a closely spaced water molecule. Possible hydrogen bonds are indicated by thin black lines and labeled by approximate distances in Å [*Permission granted*].

The protein environment surrounding the Chl a612 has to be taken into account when trying to achieve a structural assignment of the potential energy model presented above (Figure 30). Generally, the Chls are bound via liganding and hydrogen bonding to the protein mainframe formed by three membrane spanning and two amphipathic α-helices. The dynamic pigment – protein interaction may generate different conformational states of the LHC II and it also may slightly modify the absorption bands of the Chls molecules shifting them for a better light - harvesting process and an efficient EET.

Chl a612 is connected through Asn 183 as the major ligand. Hydrogen bonds are formed also between Glu and Lys residues and the closest water molecules labelled by their approximate bond length in Figure 27. An interesting fact is that the charged Lys 179 residue forms bonds with three different Chl groups of Chl a612 but also with a Glu residue. Therefore, we can assume that the presence of charged Lys residue affects the Chl site energy and may thus produce strong temperature dependence of the Chl a612 absorption band. We could say that the temperature dependence can be described by the bi- or tri-stable configuration in the neighbourhood of Chl a612 represented by the potential energy model explained in Chapter 4.2.

In summary, the lowest energy level in LHC II at low temperature (below 75 K) is believed to be located on the terminal emitter which behaves as an isolated molecule. At higher temperatures, however, the lowest excited state appears to be delocalized on three excitonically coupled Chls including Chl a612. The observation of a temperature-dependent shift of the absorption band of Chl a612 may explain these seemingly contradictory observations in the literature.

Acknowledgements

First of all, I would like to thank my supervisor Prof. Jörg Pieper for helping me throughout my thesis from who I learned a lot. One could not wish for a better supervisor.

I would also like to give thanks to: Laura Wilk in the laboratory of Prof. Werner Kühlbrandt at the Max-Planck-Institute Frankfurt, Germany, for preparation of the reconstituted LHC II and LHC II mutants; Prof. Dr. Margus Rätsep in the laboratory of Prof. Arvi Freiberg at the University of Tartu for helping me to carry out CD and ΔFLN measurements; Prof. Ivo Leito for creating and administering the program.

I would like to thank all my course mates for making my study time in Tartu interesting. Finally, I would like to thank my family for unconditional support throughout my studies in Tartu.

Summary

Photosynthesis is a key biological process on our planet. Light harvesting and excitation energy transfer are the primary processes in photosynthesis. These functions are fulfilled in green plants by photosynthetic antenna systems embedded into the thylakoid membranes on the chloroplasts.

In my thesis I am studying energy level structure and electron – phonon coupling in the light – harvesting complex II, which is one of the most abundant pigment – protein complex in green plants. I will address these problems using site selective spectroscopic techniques (Delta Fluorescence Line Narrowing and Spectral Hole Burning) and Circular Dichroism.

The ΔFLN technique has been used in the present thesis to provide insights into electron – phonon coupling of coupled Chls in monomeric Lhcb1 sample and two other mutant samples Chl a610 and Chl a612. Also it has been compared with SHB technique from the point of view of the accuracy of the information in extracting the S – factor values (the measure of electron – phonon strength) for our pigment - protein complex.

I have showed that the electron – phonon coupling strengths values calculated were closer to the real value in the low – fluence range for ΔFLN comparing with SHB results which were significant far from the true value of 1. Later we have demonstrated that the Huang – Rhys factor also depends not only on the excitation within the IDF and fluence, but also on the excitation wavelength.

Circular Dichroism spectra are due to the short – range excitonic coupling between chromophores. The removal of one of the chlorophylls from the complex affects the excitonic coupling. The temperature dependence spectrum of mutant samples show a shift from the expected linear dependence of the peaks. For Chl a612 mutant (thought to be the lowest energy state of the LHC II) we could see a strong shift of the ~680 nm peak towards red region of the spectra. A structural transition might be possible to occur over ~240 K.

The temperature dependence of the system can be described by an asymmetric double well potential, where these describes two energetically inequivalent protein conformations. The system is trapped at one conformation at low temperatures and another conformation is found at elevated temperatures.

As conclusion, the protein environment might "fine – tune" the site energies of pigment molecules.

I strongly believe that continuing researching in this area could be very interesting in finally solving one of the nature's best kept secrets, photosynthesis. We could learn from the efficiency of EET which is 99% and build artificial solar cells with increased performance.

Summary in Estonian/ Kokkuvõte

Fotoüntees on üks peamisi bioloogilisi protsesse planeedil Maa. Valguse kogumine ja ergastusenergia ülekanne on esmased protsessid fotosünteesis. Neid funktsioone täidetakse roheliste taimede poolt antennikompleksides, mis asetsevad kloroplasti tülakoidmembraanis.

Antud magistritöös olen uurinud energiatasemete struktuuri ja elektron–foonon vastasmõju valgust koguvas kompleksis II, mis on üks kõige enam esinev pigment – proteiini kompleks rohelistes taimedes. Uurin neid aspekte selektiivspektroskoopia (diferentsiaalne fluorestsentskitsenemine,ΔFLN, ja spektraalsälkamine, SHB) ja ringdikroismi (CD) meetoditega.

ΔFLN meetodit on kasutatud antud magistritöös, et saada ülevaade elektron–foonon vastasmõju tugevusest (mida iseloomustab Huang-Rhys faktor, S) kolmes proovis : monomeerne Lhcb1 ja mutantsed Chl a610 ja Chl a612. ΔFLN meetodit on võrreldud SHB meetodiga, et näha, milline meetod annab täpsema tulemuse antud pigment–proteiin kompleksides.

Olen välja toonud, et arvutatud elektron–foonon vastasmõju tugevuse väärtused madala kiiritusdoosi puhul olid ΔFLN andmete kohaselt lähedased väärtusele S=1. SHB spektrist arvutatud S-faktorid olid aga märgatavalt erinevad sellest väärtusest. Seejärel olen demonstreerinud, et Huang-Rhys faktorid sõltuvad kiiritusdoosist ja ka ergastava valguse lainepikkuse asukohast mittehomogeense jaotusfunktsiooni IDFsees.

Ringdikroismi spektrid on põhjustatud eksitoonsest vastasmõjust kromofooride vahel. Olen näitanud, et ühe klorofülli eemaldamine mõjutab eksitoonset vastasmõju. Mutantse proovi CD spektri maksimumide sõltuvus temperatuurist erineb eeldatud lineaarsest käitumisest. Temperatuuril üle 240 K ning ~680 nm maksimumi juures toimub Chl a612 mutandi tugev nihe punaste lainepikkuste suunas. See võib olla põhjustatud struktuursetest muutustest pigment–proteiin kompleksis.

Arutlesin asümmeetrilise kahe miinimumiga potensiaalse energia mudeli üle. Süsteemil on üks võimalik konformatsioon madalatel temperatuuridel ja teine kõrgetel temperatuuridel. Seega, proteiinil on võime peentimmida pigmentide energiatasemeid.

Ma usun, et uurimustöö jätkamine selles valdkonnas on huvitav ja kasulik. Võiksime õppida rohkem EET efektiivsusest, mis on 99% ja ehitada tõhusamaid kunstlikke päikeseelemente.

Bibliography

1) Amerongen, H., Valkunas, L. & Grondelle, R., 2000. Photosynthetic Excitons. *World Scientific Publishers.*

2) Arvamaa, R. & Rebane, K., 1985. High - resolution optical - spectra of chlorophyll molecules. *Spectrochimica Acta A,* Volume 41, pp. 1365 - 1380.

3) Fromme, P., 2008. *Photosynthetic Protein Complexes.* Weinheim: Willey - Blackwell.

4) Garab, G. & Amerongen, H., 2009. Linear dichroism and circular dichroism in photosynthesis research. *Photosynth Res.*

5) Gorokhovskii, A. A., Kaarli, R. K. & Rebane, L. A., 1974. *JETP Lett.,* Volume 20, p. 216.

6) Grondelle, R. & Novoderezhkin, V. I., 2005. Energy transfer in photosynthesis: experimental insights and quantitative models. *Phys. Chem. Chem. Phys.,* pp. 793 - 807.

7) Jankowiak, R., Hayes, J. M. & Small, G. J., 1993. Spectral Hole - Burning in Amorphous Molecular Solids and Proteins. *Chem. Rev.,* pp. 1471 - 1502.

8) Johnson, M. et al., 2011. Photoprotective Energy Dissipation Involves the Reorganization of Photosystem II Light - Harvesting Complexes in the Grana Membranes of Spinach Chloroplasts. *The Plant Cell*, 4 April, pp. 1468 - 1479.

9) Kharlamov, B. M., Personov, R. I. & Bykovskaya, L. A., 1974. Stable "gap"in absorption spectra of solid solutions of organic molecules by laser irradiation. *Opt. Commun,* 12(2), p. 191.

10) Kühlbrandt, W., Wang, D. N. & Fujiyoshi, Y., 1994. Atomic model of plant light-harvesting complex by electron crystallography. *Nature,* Volume 367, p. 614 .

11) Lichtenthaler, L., 1987. Chlorophylls and carotenoids: Pigments of photosynthetic biomembranes. In: *Methods in Enzymology.* s.l.:s.n., pp. 350 - 382.

12) Liu, Z. et al., 2004. Chrystal structure of spinach major light - harvesting complex at 2.27 Å resolution. *Nature,* pp. 287 - 292.

13) Müh, F., Madjet, M. E.-A. & Renger, T., 2010. Structure - Based Identification of Energy Sinks in Plant Light - Harvesting Complex II. *J. Phys. Chem.,* pp. A - R.

14) Pieper, J. & Freiberg, A., In press. Electron - Phonon and Exciton - Phonon Coupling in Light Harvesting, Insights from Line - Narrowing Spectroscopies. In: s.l.:s.n.

15) Pieper, J., Rätsep, M., Irrgang, K.-D. & Freiberg, A., 2009. Chromophore - Chromophore and Chromophore - Protein Interactions in Monomeric Light - Harvesting Complex II of Green

Plants Studied by Spectral Hole Burning and Fluorescence Line Narrowing. *J. Phys. Chem.,* pp. A - K.

16) Pieper, J. et al., 2011. Excitonic Energy Level Structure and Pigment-Protein Interactions in the Recombinant Water-Soluble Chlorophyll Protein.I. Difference Fluorescence Line-Narrowing. *The Journal of Physical Chemistry B.*

17) Reppert, M., Naibo, V. & Jankowiak, R., 2010. Modeling study of non-line-narrowed hole-burned spectra in weakly coupled dimers and multi-chromophoric molecular assemblies. *J. Chem. Phys.,* Volume 367, pp. 27 - 35.

18) Rogl, H. & Kühlbrandt, W., 1999. Mutant trimers of light - harvesting complex II exhibit altered pigment content and spectroscopic features. *Biochemistry,* pp. 16214 - 16222.

19) Rogl, H. et al., 2002. Assignment of Spectral Substructures to Pigment - Binding Sites in Higher Plant Light - Harvesting Complex II. *American Chemical Society, Biochemistry,* pp. 2281 - 2287.

20) Ruban, A. V., 2012. The Photosynthetic Membrane: Molecular Mechanisms and Biophysics of Light Harvesting. In: s.l.:John Wiley & Sons.

21) Standfuss, J. & Kühlbrandt, W., 2004. The Three Isoforms of the Light - Harvesting Complex II. *The Journal of Biological Chemistry,* pp. 36844 - 36891.

22) Standfuss, J., Scheltinga, A. C. T., Lamborghini, M. & Kühlbrandt, W., 2005. Mechanisms of photoprotection and nonphotochemical quenching in pea light - harvesting complex at 2.5 Å resolution. *The EMBO Journal,* pp. 1 - 10.

23) Theiss, C. et al., 2011. Excitation energy transfer in intact cells and in the phycobiliprotein antennae of the chlorophyll d containing cyanobacterium Acaryochloris marina. *Journal of Plant Physiology,* pp. 1473 - 1487.

24) Vrandecic, K., 2013. Energy level structure and protein dynamics in the light - harvesting complex II. *MSc Thesis.*

25) Vrandecic, K. et al., not published, 2014. Protein dynamics tunes excited state positions in light - harvesting complex II.

Appendix 1

Fitting parameters I used to model the shape of the absorption bands for all three samples used (a part of fitting data). Figures and the S – factors extracted are presented in Chapter 3.2

Lhcb1	Excitation wavelength 680nm						
Fluence	32 J/cm²	16 J/cm²	8 J/cm²	4 J/cm²	2 J/cm²	1 J/cm²	0.5 J/cm²
phfreq1	15	15	15	15	15	15	15
hr1	0.58	0.46	0.46	0.44	0.42	0.41	0.41
gssphwdt1	23	18	18	18	18	18	18
ltzphwdt1	48	48	48	48	48	48	48
phfreq2	62	60	60	60	60	60	60
hr2	0.35	0.31	0.31	0.31	0.31	0.32	0.32
gssphwdt2	70	70	70	69	70	70	70
ltzphwdt2	54	54	54	54	54	54	54
phfreq3	110	110	110	110	110	110	110
hr3	0.16	0.1	0.1	0.1	0.1	0.1	0.1
gssphwdt3	60	60	60	60	60	60	60
ltzphwdt3	30	38	38	38	38	38	38
zplpeak	0	0	0	0	0	0	0
zplwdt	2.3	2.2	2.2	2.2	2.2	2.2	2.2

hr1	hr2	hr3	Total S-factor
0.58	0.35	0.16	1.09
0.5	0.35	0.15	1
0.47	0.34	0.14	0.95
0.46	0.34	0.14	0.94
0.42	0.33	0.13	0.88
0.42	0.33	0.13	0.88
0.42	0.33	0.13	0.88

Fluence [J/cm²]	Total S-factor
32	1.09
16	1
8	0.95
4	0.94
2	0.88
1	0.88
0.5	0.88

Excitation Wavelength	S-factor
680	0.88
682	0.83
684	0.82
686	0.81
688	0.81
690	0.81

Chl *a*612	Excitation wavelength 680nm					
	32	16	8	4	2	1	0.5
Fluence	J/cm²	J/cm²	J/cm²	J/cm²	J/cm²	J/cm²	J/cm²
phfreq1	20	20	20	20	20	20	20
hr1	0.53	0.51	0.5	0.49	0.48	0.46	0.45
gssphwdt1	26	25	24	22	22	22	22
ltzphwdt1	44	44	44	44	44	44	44
phfreq2	62	62	62	62	62	62	62
hr2	0.26	0.24	0.22	0.22	0.22	0.22	0.22
gssphwdt2	50	48	46	46	46	46	46
ltzphwdt2	54	54	54	54	54	54	54
phfreq3	110	110	110	110	110	110	110
hr3	0.14	0.14	0.12	0.12	0.12	0.12	0.12
gssphwdt3	62	62	62	62	62	62	62
ltzphwdt3	40	40	40	40	40	40	40
zplpeak	0	0	0	0	0	0	0
zplwdt	2	2.2	2.2	2.2	2.2	2.2	2.2

hr1	hr2	hr3	Total S-factor
0.53	0.26	0.14	0.93
0.51	0.24	0.14	0.89
0.5	0.22	0.12	0.84
0.49	0.22	0.12	0.83
0.48	0.22	0.12	0.82
0.46	0.22	0.12	0.8
0.45	0.22	0.12	0.79

Fluence [J/cm²]	Total S-factor		Excitation wavelength	S-factor
32	0.93		680	0.79
16	0.89		682	0.93
8	0.84		684	0.81
4	0.83		686	0.78
2	0.82		688	0.82
1	0.8			
0.5	0.79			

Chl a610	Excitation wavelength 678nm						
	32	16	8	4	2	1	0.5
Fluence	J/cm²	J/cm²	J/cm²	J/cm²	J/cm²	J/cm²	J/cm²
phfreq1	18	18	18	18	18	18	18
hr1	0.61	0.57	0.52	0.47	0.43	0.41	0.41
gssphwdt1	26	26	26	27	28	28	28
ltzphwdt1	42	42	42	42	42	42	42
phfreq2	62	62	62	62	62	62	62
hr2	0.38	0.38	0.33	0.32	0.29	0.28	0.27
gssphwdt2	54	54	54	54	54	50	50
ltzphwdt2	54	54	54	54	54	54	54
phfreq3	110	110	110	110	110	110	110
hr3	0.14	0.12	0.11	0.1	0.1	0.1	0.1
gssphwdt3	62	62	62	62	62	62	62
ltzphwdt3	40	40	40	40	40	40	40
zplpeak	0	0	0	0	0	0	0
zplwdt	2.3	2.3	2.3	2.3	2.3	2.3	2.3

hr1	hr2	hr3	Total S-factor
0.61	0.38	0.14	1.13
0.58	0.38	0.12	1.08
0.52	0.33	0.11	0.96
0.47	0.32	0.1	0.89
0.43	0.29	0.1	0.82
0.41	0.28	0.1	0.79
0.41	0.27	0.1	0.78

Fluence [J/cm²]	Total S-factor		Excitation wavelength	S-factor
32	1.13		678	0.78
16	1.08		680	0.72
8	0.96		682	0.85
4	0.89		684	0.87
2	0.82			
1	0.79			
0.5	0.78			

Non-exclusive licence to reproduce thesis and make thesis public

I, _____Petrică Artene_____

(Author's name)

(Date of birth: _____28.06.1986_____),

1. Herewith grant the University of Tartu a free permit (non-exclusive licence) to:

1.1. reproduce, for the purpose of preservation and making available to the public, including addition to the DSpace digital archives until expiry of the term of validity of the copyright, and

1.2. make available to the public in the web environment of the University of Tartu, including the DSpace digital archives until expiry of the term validity of the copyright,

(Title of thesis)

"Energy level structure and electron – phonon coupling in the light – harvesting complex II"

Supervised by _____Prof. Dr. Jörg Pieper_____,

(Supervisor's name)

2. I am aware of the fact that the author retains these rights.

3. I certify that granting the non-exclusive licence does not infringe the intellectual property rights or rights arising from the Personal Data Protection Act.

Tartu, 02.06.2014